This is a repository copy of *Benefits of spanwise gaps in cylindrical vortex generators for conjugate heat transfer enhancement in micro-channels*.

Version: Accepted Version

Accepted Manuscript

Benefits of spanwise gaps in cylindrical vortex generators for conjugate heat transfer enhancement in micro-channels.

Mushtaq T. Al-Asadi, Fahad S. Alkasmoul, Mark C.T. Wilson

Please cite this article as: M.T. Al-Asadi, F.S. Alkasmoul, M.C.T. Wilson, Benefits of spanwise gaps in cylindrical vortex generators for conjugate heat transfer enhancement in micro-channels., *Applied Thermal Engineering* (2017), doi: https://doi.org/10.1016/j.applthermaleng.2017.10.157

Benefits of spanwise gaps in cylindrical vortex generators for conjugate heat transfer enhancement in micro-channels.

Mushtaq T. Al-Asadi*[a, b], Fahad S. Alkasmoul[c], Mark C. T. Wilson*[a]

[a]*Institute of Thermofluids, School of Mechanical Engineering, University of Leeds, UK.*

[b]*Refrigeration Department, Eng. Division, Basra Oil Company, Ministry of Oil, Basra, Iraq.*

[c] *King Abdulaziz City for Science and Technology in Riyadh, Saudi Arabia.*

Abstract

Cylindrical vortex generators placed transversely over the span of a micro-channel can enhance heat transfer performance, but adding full-span vortex generators incurs a substantial pressure drop penalty. This paper examines the benefits of introducing various gaps along the length of the vortex generators, both for reducing pressure drop and improving the thermal conductance of the system. Three particular configurations are considered with varied dimensions: symmetrical gaps at each end of the vortex generator, i.e. adjacent to the channel side walls; a single central gap; and a combination of a central and end gaps. The performance is investigated numerically via 3D finite element analysis for Reynolds number in the range 300-2300 and under conditions of a uniform heat flux input relevant to microelectronics cooling. Results demonstrate that having end gaps alone substantially improves heat transfer while reducing the pressure drop. As well as generating longitudinal vortices which draw heat from the adjacent channel side walls, hot fluid passing through the gaps is swept directly upwards and inwards into the bulk flow, where it remains as it flows to the outlet. A thermal-hydraulic performance evaluation index is improved from 0.7 for full-span vortex generators to 1.0 with end gaps present. The central and central-plus-end gap geometries are less effective overall, but do offer localised improvements in heat transfer.

---

*Corresponding author, email:

ml13mtka@leeds.ac.uk (M. T. Al-Asadi), M.Wilson@leeds.ac.uk (Mark C. T. Wilson)

Nomenclature

A_s	surface area of the whole heat sink (μm^2)	r	radius of VGs, μm
CFD	Computational Fluid Dynamics	Re	Reynolds number
C_p	Specific heat, J/Kg.K	T	Temperature, K
D	Diameter, μm	X	Axial distance, μm
FEM	Finite Element Method	**Greek Symbols**	
FVM	Finite Element Method	μ	Viscosity, Pa.s
K	Thermal conductivity, W/m.K	Θ	Thermal resistance, K/W
L	Channel length, μm	ρ	Densities, kg/m^3
VGs	Vortex generators	**Subscripts**	
P	Pressure, N/m^2	ave	Average
		In	Inlet
		max	Maximum
		Out	Outlet
		S	Surface
		L	Liquid

q   Uniform heat flux, W/cm^2

1. Introduction

Thermal management is becoming increasingly important especially with the rapid minimization of electronic chips, which continues to provide challenges for thermal researchers. Indeed, reduction in chips size is a real challenge for designing efficient cooling systems with limited space in which to reject generated heat [1-4]. One of the promising systems by which high performance heat rejection can be achieved is micro and mini-scale systems, such as micro-channel heat exchangers and heat sinks [5-9]. They are different from traditional channels, and can be classified according to their associated hydraulic diameters, D_h, [10-12].

Work on micro-channels has developed since 1981 when the novel idea of shrinking the hydraulic diameter, D_h, was presented to produce an efficient micro-channel with greater capability to reject the generated heat [13]. From an analysis perspective, a key feature of micro-channels is that the hydraulic diameter becomes comparable with the channel wall thicknesses, and consequently in transverse cross-sections of micro-channel heat sinks, the area of the solid material is commensurate with the fluid area [14]. This means that conjugate heat transfer phenomena such as axial conduction in the solid must be accounted for, and boundary conditions applied at channel walls based on Nusselt number correlations from larger channels can lead to inaccurate results [15].

Since experimental measurements of local heat fluxes and wall temperatures are impossible or very difficult in microscale systems, numerical analyses of conjugate heat transfer have been useful in interpreting experimental data and studying deviations of micro-channel behavior from conventional laws [16]. Koşar [9] used COMSOL Multiphysics® to perform conjugate heat transfer analysis on various micro-channels to establish a new Nusselt number correlation suitable for applying a constant heat flux boundary condition, together with a new dimensionless parameter and associated criteria to indicate system conditions under which the boundary condition is appropriate.

As full three-dimensional numerical analysis of conjugate heat transfer can be computationally demanding and time consuming, several alternative approaches have been developed. Nonino *et al.* [14] studied circular micro-channels using an axisymmetric model in which the velocity field is pre-computed from the parabolized Navier-Stokes equations and mapped onto a two-dimensional mesh for the energy equation. This was applied to illustrate the influences of channel end effects, wall thickness and axial conduction on the temperature distributions and Nusselt number. Knupp *et al.* [15] used a generalized integral transform technique to solve merged fluid-solid energy equations in a single domain

2

describing two-dimensional conjugate heat transfer between parallel plates representing channels with very high walls compared to the channel width.

To meet the rapid developments in electronics chips, various augmentations of micro-channel heat sinks have been explored to enhance their performance further. Hong et al. [17] sought to improve the uniformity of temperature distribution in micro-channel heat sinks by considering a heat sink in which the micro-channels formed a rectangular fractal-shaped network. Their numerical analysis of the 3D conjugate heat transfer revealed hotspots in regions where the channel density was sparse, but these could be overcome by local modifications of the channel size. The modified network was found to have lower thermal resistance, lower pressure drop and much improved uniformity in temperature compared to parallel-channel heat sinks.

Other ideas have focused on modifications the parallel channels themselves, for example by adding grooves or ribs [18-21]. They act as vortex generators (VGs) to enhance heat transfer and fluid flow characteristics by disturbing the flow and creating vortices that can been classified as transverse vortices, where the axis of rotation is perpendicular to the flow direction, or longitudinal vortices, with axes lying along the direction of flow. Generally, longitudinal vortices are more effective than transverse ones in enhancing heat transfer performance [22-24]. VGs can take various forms such as protrusions, wings, inclined blocks, winglets, fins, and ribs [25-28], and have also been used to enhance heat transfer in different geometries such as circular and non-circular ducts under turbulent flow [29-31]. They have also been used in laminar flow [32], with flat plate-fins in rectangular channels [33-35], tube heat exchangers [36], heat sinks [32, 37] and rectangular narrow channels [38, 39].

Xia et al. [40] reported that the rectangular micro-channel was the best geometry among various micro-channel shapes. VGs enhanced the Nusselt number up to 25% in a study by Ebrahimi et al. [25] with Reynolds number, Re, in the range of 100-1100. However, the friction factor increased by up to 30% when using the VGs. Other recent investigations have also indicated potential benefits of using VGs of various shapes with laminar flow at different Reynolds number [38, 41, 42].

The present work is focused on cylindrical or rib-based structures, which have received some recent attention. A 2D numerical study by Cheraghi et al. [6] investigated the impact of the position of an adiabatic cylinder in a uniform micro-channel. They used fixed heat flux applied to the wall sides, Reynolds number of 100 and the Prandtl number ranged from 0.1 to 1. It was found that the maximum heat transfer enhancement occurred when the cylinder was fixed in the halfway position from the bottom of the uniform channel. The results also

3

showed that the low Prandtl number had a positive effect on heat transfer enhancement. Another study using cylindrical vortex generators under turbulent flow is that of Wang and Zhao [43], who found that utilizing a cylindrical VGs enhanced the heat transfer by 1.18 times compared to the uniform channel.

Chai et al. [44] investigated numerically the effects of ribs on the side walls of a silicon micro-channel heated from below and cooled by laminar water flow. The ribs were arranged in an offset manner on both side walls, and had various cross-sectional shapes, namely rectangular, backward triangular, forward triangular, isosceles triangular and semicircular, each with a protrusion of 25 μm into the channel. For Reynolds number in the range 190-838, Nusselt numbers up to 1.95 times that of a smooth channel were achieved, with the apparent friction factor increasing up to 4.57 times. Performance evaluation criteria values of 1.02 to 1.48 were found, with forward triangular ribs performing best for Re < 350, and semicircular ribs for Re > 400. In a further three-part work, the same authors also studied aligned versus offset fan-shaped ribs on the opposite side walls [45-47]. Various other side-wall rib shapes and configurations have also been considered by others, e.g. [2, 27] .

A recent 3D conjugate heat transfer investigation by Al-asadi et al. [48] studied the influence of cylindrical VGs placed on the base of a micro-channel rather than the side walls. In particular, they considered VGs with quarter- and half-circular cross-sections of radii up to 400 μm mounted at intervals on the base of the microchannel, aligned perpendicular to the flow direction, with an input heat flux in the range of 100-300 W/cm^2 and Reynolds number ranging from 100 to 2300. While the quarter-circle VGs offered no improvement in heat transfer, the half-circle cylindrical VGs did result in a reduced thermal resistance of the system. In addition to VGs completely spanning the width of the microchannel, shorter VGs were also considered. It was found that having a gap between each channel wall and the ends of the VGs offered further heat transfer benefits, particularly when the pressure drop penalty was taken into account. However, the underlying mechanisms by which the gaps enhance performance were not explored, and only one end gap size was considered.

This paper builds on that previous work [48] to identify the mechanism of heat transfer enhancement, to explore the effect of the end gap width and determine the optimum size, and to investigate different gap configurations not considered previously. The study is also extended to assess the effects of VG radius, position, number and material. Section 2 describes the geometry in more detail, after which Section 3 discusses the mathematical model and Section 4 the numerical approach and validation process. The main results are discussed in Section 5, and conclusions are drawn in Section 6.

4

2. Micro-channel and vortex generator geometry

The application considered is a micro-channel heat sink, with a base area $A_s = 6.25 \times 10^8$ μm², suitable for use in cooling a microprocessor chip. The coolant used is water. For modelling purposes, a single rectangular uniform micro-channel is taken as a reference design as presented in Fig 1(f). Within this channel, five cylindrical VGs with a half-circle cross-section are added at uniform (4000 μm centre-to-centre) intervals along the base of the channel and aligned perpendicular to the flow. The VGs do not fully span the width of the channel; they have gaps of variable width at different locations as indicated in Fig. 1(b-d). Three specific configurations are considered: a 'central' gap (Fig. 1b) located in the middle of the channel width, 'end' gaps (Fig. 1c) located between each end of the VG and the nearby channel side wall, and a combination of both end gaps and a central gap (Fig. 1d). These configurations will be referred to by the codes 'C', 'E' and 'CE' as indicated in Table 1, which also gives the relevant dimensions.

The micro-channel dimensions were derived from considering a heat sink comprising 30 channels fitted to a CPU chip with a surface size of 25 × 25 mm. The sizes of the VGs were selected to provide a range of sizes that fit within the resulting channel. It is acknowledged that manufacturing heat sinks with such VGs, especially with narrow gaps, could be challenging. However, the geometries are simpler than many examples considered in the literature, and manufacture could be possible for example using CNC laser cutting.

3. Mathematical modelling

3.1 Governing equations

The coolant in the channel is taken to be water, with temperature-dependent density ρ and viscosity μ, flowing under steady laminar conditions. Gravitational effects are not important in this small, closed-domain forced convection system and, since water is Newtonian, the governing continuity and Navier-Stokes equations therefore take the form:

$$\nabla \cdot (\rho \boldsymbol{u}) = 0 \tag{1}$$

$$\rho(T_L)(\boldsymbol{u} \cdot \nabla)\boldsymbol{u} = \nabla \cdot \left[-p\boldsymbol{I} + \mu(T_L)(\nabla \boldsymbol{u} + (\nabla \boldsymbol{u})^T) - \frac{2}{3}\mu(T_L)(\nabla \cdot \boldsymbol{u})\boldsymbol{I} \right], \tag{2}$$

where $\boldsymbol{u} = (u, v, w)$ is the flow velocity in (x, y, z) Cartesian coordinate space, and p is the pressure. The energy equation for the water is

$$\rho C_p \boldsymbol{u} \cdot \nabla T_L = \nabla \cdot (k \nabla T_L) \tag{3}$$

where C_p, T_L, and k are respectively the specific heat, temperature, and thermal conductivity of the liquid. Viscous dissipation is neglected since water viscosity is low. The solid parts of the domain are taken to be aluminium, since this is a common material from which heat

5

sinks are made, though some results for copper are also presented below. Heat conduction through the solid is governed by

$$\nabla \cdot (k_S \nabla T_S) = 0 \tag{4}$$

where T_S and k_S are respectively the temperature and thermal conductivity of the solid. The temperature dependence of the fluid properties is given by the following expressions built in to COMSOL based on experimental data:

$$\rho(T_L) = 838.466135 + 1.40050603 T_L - 0.0030112376 T_L^2 + 3.71822313 \times 10^{-7} T_L^3$$

$$\mu(T_L) = 1.3799566804 - 0.021224019151 T_L + 1.3604562827 \times 10^{-4} T_L^2$$
$$- 4.6454090319 \times 10^{-7} T_L^3 + 8.9042735735 \times 10^{-10} T_L^4$$
$$- 9.0790692686 \times 10^{-13} T_L^5 + 3.8457331488 \times 10^{-16} T_L^6$$

$$C_p(T_L) = 12010.1471 - 80.4072879 T_L + 0.309866854 T_L^2$$
$$- 5.38186884 \times 10^{-4} T_L^3 + 3.62536437 \times 10^{-7} T_L^4$$

$$k(T_L) = -0.869083936 + 0.00894880345 T_L - 1.58366345 \times 10^{-5} T_L^2 + 7.97543259 \times 10^{-9} T_L^3$$

3.2 Boundary conditions

As indicated in Fig. 1(e), the symmetry of the flow was exploited to reduce computational effort, and symmetry conditions were applied at the left- and right-hand outer boundaries of the domain, corresponding to the centre of the channel and the centre of the wall between two channels respectively. A uniform heat flux was applied at the bottom boundary, as an idealised representation of a live CPU chip requiring cooling via the heat sink. It is assumed that the micro-channels in the heat sink are fed from a header chamber, so at the micro-channel inlet a uniform velocity was imposed. The inlet speed u_{in} was set to achieve the desired Reynolds number, defined in terms of the hydraulic diameter as

$$Re = \frac{\rho u_{in} D_h}{\mu}. \tag{5}$$

The inlet temperature was fixed at 293.15 K. At the outlet, the pressure was set to zero, and on the micro-channel walls the no-slip condition was applied. On the top boundary, and the remaining walls, adiabatic conditions were applied. Table 2 summarises the boundary conditions together with the relevant equations.

3.3 Heat transfer performance characterisation
The heat transfer performance is quantified by the thermal resistance, defined as

6

$$\theta = \frac{T_{ave} - T_{in}}{A_s q}, \tag{6}$$

where T_{ave} is the average temperature in the system, T_{in} is the inlet temperature, and q is the heat flux through the base of the heat sink. A thermal-hydraulic performance evaluation criteria (PEC) index [18, 19] is also used to assess the effective heat transfer enhancement provided by VGs, taking into account the penalty paid in terms of the pressure drop. Rather than using the usual average Nusselt numbers and friction factors as the contrasted thermal and hydraulic measures [18, 19], here the PEC index is defined in terms of equivalent directly computed quantities, namely the thermal conductance of the system (i.e. the reciprocal of the thermal resistance) and the actual pressure drop. Hence the PEC index is defined as:

$$\text{PEC} = \frac{\theta_s/\theta}{(\Delta P/\Delta P_s)^{1/3}} \tag{7}$$

where ΔP and θ are the pressure drop and thermal resistance in a microchannel containing VGs and ΔP_s and θ_s are the same quantities in the corresponding smooth (i.e. uniform) micro-channel. (Note a typographical error in the equivalent equation presented in our previous paper [48] – the equation should be as it appears here.)

4. Numerical method, mesh, and code validation

The governing equations (1)-(4) were solved numerically using the finite element method via the COMSOL Multiphysics® version 5.1 software package. A grid independence study was conducted to assess the number of elements required for accurate but efficient solutions. The details of this have been published previously [48] and are not reproduced here, except to note that a difference of less to 0.01% was observed in corresponding average and maximum temperatures calculated on the 'fine' mesh (with 788230 elements, used for results presented here) and the 'finer' mesh (with 2831904 elements). Good agreement was also seen with relevant previous work, again as reported by Al-Asadi et al. [48].

To validate the computational approach against experimental data, comparisons are here made with the experimental investigation of a straight micro-channel by Kawano et al. [49]. Comparisons are also made with a numerical study of the same system by Qu and Mudawar [50]. Both studies used the same material, namely silicon, and the dimensions of the micro-channel were 180 μm, 57 μm, 10mm in height, width and the length, respectively. The top of micro-channel was subjected a uniform heat flux of 90 W/cm², while the side walls were set to be symmetry planes, and an adiabatic condition was imposed on the bottom wall. Laminar flow was utilized in the studies with Reynolds number ranging from 80 to 400. Fig. 2

7

presents the thermal resistance calculated as $R_{th,\ out}= (T_{surface,\ Max}-T_{fluid,\ in}/\ q)$ and shows excellent agreement between the present numerical results and the experimental data; in fact the thermal resistance obtained agrees a little more closely than that of Qu and Mudawar [50], particularly at the higher end of the available Reynolds number range. Hence the computational approach used here is considered to be sufficiently reliable.

5. Results and discussion

In this study, three-dimensional laminar flow simulations were conducted with Reynolds number in the range 300-2300 to assess the effects of the various gaps in the VGs (described in Sec. 2) on the conjugate heat transfer, with water as the working fluid. The results presented below focus on the particular value of 100 W/cm^2 for the heat flux, because this corresponds to the upper limit for operation of electronic devices [51-53]. There is a very large parameter space associated with the VG geometry: in addition to the gap positions and widths of primary interest, other parameters include the radii, longitudinal position, separation and number of VGs, as well as the conductivity of the VG and channel material. These will be considered in sub-sections below, but to begin we consider the same VG arrangement used in our previous paper [48], namely a series of 5 equally-spaced aluminium VGs of radius 400 µm.

5.1 End gaps (E-type vortex generators)

Our previous study [48] showed that centred VGs shorter than the full span of the channel provided a lower thermal resistance and lower pressure drop than full-span VGs. In other words, having a gap between the ends of the VG and the channel side walls is beneficial. However, only one size of end gap was considered in that work, and the mechanism by which the modified flow enhanced performance was not explored. Therefore the starting point for the results presented here is an investigation of how the width of the end gaps affects the performance of the system, to see if there is an optimum gap.

5.1.1 The effect of end-gap width on thermal resistance and pressure drop

Fig. 3 shows how the thermal resistance (6) and the pressure drop along the channel vary with Reynolds number for a selection of different end-gap widths. Note that the gap size given in the legend refers to the combined width of the symmetrical gaps at each end. For clarity, not all gap sizes from Table 1 are shown. The gap size considered previously [48] is here labelled as 'E3' and consists of a 100 µm gap at each end of the VG. It is found that

8

this gap width produces a lower thermal resistance than all larger gap widths, but inevitably does result in a greater pressure drop than VGs with larger gaps. However, it is possible to reduce the thermal resistance a little more by decreasing the gap further, as the curve for the E2 model (two 75 µm gaps) shows. Of course the pressure drop is increased, but the E2 pressure drop is still less than that for full-span VGs that have a much higher thermal resistance.

Reducing the gap size further than E2 does not provide any benefit. For example, the E1 VGs (two 25 µm gaps) produce the same thermal resistance as E2 VGs (not shown in Fig. 3 for clarity), but a much higher pressure drop. In fact this pressure drop (see Fig. 3) actually exceeds that for full-span VGs, as a result of the higher viscous drag caused by the very narrow gaps. Such small gaps would also be more challenging to manufacture. In terms of the achievable thermal resistance, the E2 VG with an overall gap of 150 µm (i.e. a 75 µm gap at each end) could therefore be considered as the optimum E-type VG, as it will produce a lower pressure drop than the VGs with the same thermal resistance but narrower gaps.

It is worth noting that the E7 VGs, which have two gaps of 200 µm each, show almost exactly the same thermal resistance as the full-span VGs, yet with a greatly reduced pressure drop. In fact the pressure drop is not much higher than for the uniform channel with no VGs present (see Fig. 3). The low pressure drop penalty is to be expected given that the gaps in the E7 VGs are 80% of the channel width.

5.1.2 Performance evaluation criteria index

In an attempt to give a quantitative indication of the benefit versus cost of having VGs present in the channel, the Performance Evaluation Criteria (PEC) index defined in equation (7) sets the relative change in the thermal conductance of the system (with respect to a uniform channel) against the relative change in the pressure drop. Fig. 4 shows the values of this index as a function of Reynolds number for a selection of end-gap widths (the legend gives the combined width of the two symmetrical gaps at each end of the VG). On this measure, the E2 VG is essentially 'neutral' for the higher Re values – i.e. its PEC values are close to unity, so its improvement in thermal conductance is in some way 'worth' the increase in pumping power required. In contrast, the PEC values for the E1 VG are rather lower, levelling out at about 0.85, consistent with the observations in the previous section that reducing the size of the end gap below that of the E2 VG simply raises the pressure drop with no improvement in thermal resistance/conductance.

Similarly, the E7 VG noted above reaches PEC values above one, since its relatively large gaps mean that the pressure drop is only a little higher than that of the uniform channel.

However, this is not the largest PEC value that can be achieved with end gaps. The highest PEC value obtained is about 1.02 with the E6 VG, having end gaps of 175 µm each. This VG does however have a rather higher thermal resistance than the E2 VG (it is not shown in Fig. 3 but has a thermal resistance slightly lower than the E7 VG).

5.1.3 Vortical flow structure and solid temperature distribution

The key effect of having a gap between the end of the VG and the channel wall, instead of a full-span VG, is that longitudinal vortices can be formed, i.e. with rotation axes parallel to the main flow direction. This can be seen clearly by tracing the 3D trajectories of passive particles in the flow, as shown in Fig. 5. A full-span cylindrical VG obviously completely blocks the flow in the lower part of the channel, and the inertia of the fluid passing over the VG results in an extended transverse vortex – i.e. with rotation axis perpendicular to the flow – see the blue trajectories in Fig. 5(a). There is also some weak large-scale rotation of the flow in the y-z plane, caused by the difference in boundary conditions at the solid side wall and symmetry plane, but the dominant effect is the transverse vortex.

With a gap present, the flow is very different and substantial longitudinal vortices arise – see the red trajectories in Fig. 5(b). Fluid which passes through the gap is swept upwards and towards the middle of the channel, as shown by the blue trajectories in Figs. 5(b) and (c), which is clearly beneficial for heat transfer from the solid surfaces of the base and side walls to the bulk fluid. Towards the middle of the VG there is still a transverse vortex element to the flow, but this is much more open than the clearly defined and essentially closed transverse recirculation behind the full-span VG seen in Fig. 5(a).

To illustrate the end gap effect on conjugate heat transfer, Fig. 6 shows temperature contours within the solid base and the solid side wall of the channel, on planes located 2 µm from the solid-water contact surfaces. The plots compare full-span VGs with E2 VGs, with the flow from right to left, at Re = 500 as in Fig. 5. The contours for the full-span (F) VGs clearly show the influence of the VGs in reducing the local solid temperature via improved heat transfer to the fluid, though there are local hotspots behind each VG, corresponding to the enclosed transverse vortices seen in Fig. 5(a). In comparison, the E2 temperature contours show a consistent approximately 5K lower temperature at corresponding points in the channel. In particular, the side-wall contours (Fig. 5b) show a reduction in the vertical extent of the hotspots, and reduced temperatures in the upper areas of the wall, consistent with the transport of fluid upwards and inwards (away from the wall) seen in Fig. 5(b).

5.1.4 The effect of VG position and number

10

The results presented above are for a series of 5 equally-spaced VGs of radius 400 μm. Clearly this is just one configuration, so here we explore the effect of changing that configuration. To illustrate the effect of VG position, we consider a channel with a single E2 VG (of radius 400 μm) and vary the position, D, of the centre of the VG from the channel inlet. Fig. 7 shows that the VG position in the channel has barely any influence on the resulting thermal resistance of the channel, and only a small effect on the pressure drop due to the development of the flow from the inlet along the channel.

Though the position of the VGs is not important, the number of VGs will clearly influence both the thermal resistance and the pressure drop. Fig. 8 shows the values of these quantities for series of 4, 5 and 6 equally-spaced E2 VGs. As to be expected, adding more VGs lowers the thermal resistance but raises the pressure drop. However, in stepping from five to six VGs, the change in thermal resistance is rather less than the change in pressure drop, indicating that the benefit of decreased thermal resistance could be outweighed by the increased pumping power required. Indeed, this is confirmed by calculating the corresponding PEC values using eq. (7), which are plotted in Fig. 9. As already observed in section 5.1.2, the series of 5 VGs has an essentially neutral PEC (i.e. close to unity), especially for higher Re, indicating that increased pressure drop is balanced by a commensurate improvement in thermal performance. The series of 4 and 6 VGs have PEC also have values that are quite high, but they are both lower than for the 5 VGs. The cost of heat transfer enhancement in terms of the pressure drop penalty is therefore slightly higher than for the 5 VGs. All the remaining results presented here correspond to a series of 5 VGs.

5.1.5 The effect of VG radius

The results presented so far are all for VGs of radius 400 μm, but Fig. 10 shows how the VG radius affects the thermal resistance and pressure drop for a series of five E2 VGs. As is to be expected, increasing the radius generally reduces the thermal resistance. This is a result of an increased solid surface area in contact with the fluid and greater penetration of the (high-conductivity) solid into the bulk flow, as well as the mixing effects of the vortices generated. An exception to this is the very small-radius (100 μm) VGs at low Reynolds numbers. In that case, the thermal resistance is actually higher than that of the uniform channel. This is because at low Re the inertia of the flow passing over these small VGs is insufficient to generate a substantial recirculating wake. Instead, the fluid immediately behind the VGs is essentially stagnant, resulting in local hotspots and the associated increase in thermal resistance.

Clearly, increasing the radius of the VGs will increase the blockage of the micro-channel resulting in an increased pressure drop along the channel. This is evident in the pressure drop curves of Fig. 10, which highlight the dramatic increase in pressure drop for large radii. Similar observations are seen for the other VG configurations considered here.

Since the radius of the VGs produces a quantitative rather than qualitative change in behaviour (except for very small radii at low Re), for illustrative purposes the remainder of the results will be presented for VG radii of 400 µm. This is a convenient value for revealing the effects of the VG gaps prominently without too excessive a pressure penalty.

5.1.6 The effect of solid thermal conductivity

As stated in section 3.1, the solid material considered here is aluminium (thermal conductivity 238 $Wm^{-1}K^{-1}$), since this is a popular and economical material used for heat sinks. However, copper is also used for heat sinks and offers a higher thermal conductivity of 400 $Wm^{-1}K^{-1}$ (as well as a higher volumetric heat capacity). To assess the effect of the solid material on the performance of the vortex generators, simulations with five E2-type VGs were repeated with copper as the solid material. Fig 11 shows a comparison of the resulting temperature distributions in the channel side wall and channel base. The higher thermal conductivity of the copper of course results in faster heat conduction through the solid, which leads to greater heat transfer to the fluid occurring further upstream than with the aluminium. The thermal boundary layers develop more rapidly with the copper, such that downstream the boundary layer is thicker and heat transfer efficiency from solid to fluid is reduced. This results in higher downstream temperatures in the copper (see Fig. 11b and c). As a consequence, the calculated thermal resistance is slightly higher for the copper micro-channel, as can be seen in Fig. 12. The pressure drop (Fig. 12) is very slightly lower for the copper case because of the higher fluid temperature and consequential reduction in fluid viscosity.

Though there are clearly small quantitative differences in the calculated performance of the aluminium and copper micro-channels, the qualitative behaviour of the VGs is the same in both cases (see for example the temperature distributions in Fig. 11). Aluminium has several practical advantages over copper including its low density, lower cost and relatively easier manufacturability.

5.2 Vortex generators with a single central gap (C-type VGs)

Having seen the benefits of having a gap at each end of the VG, the effect of a single central gap is now assessed. Fig. 13 shows the corresponding thermal resistance and the pressure

12

drop obtained for various gap widths, and compares this with the performance of the uniform channel and a channel with full-span cylindrical vortex generators present. For very wide gaps, the thermal resistance is similar to that of the uniform channel. As the gap is reduced, which is equivalent to extending two short VGs from each channel wall, the thermal resistance decreases. However, the change is not monotonic. For example, at $Re < 900$ the VGs with a 400 μm gap perform better than those with a 450 μm gap, but for larger Re the opposite is true. As in the case of small VG radii discussed in section 5.1.5, this is because at low Reynolds numbers the inertia of the flow is too weak to generate a substantial eddy behind the very short solid parts of the VGs. Improvement in heat transfer is primarily due to the increase in surface area and thermal bridging effect of the higher conductivity solid. As Reynolds number and/or length of the VG increases, the additional benefit of the enhanced vortices leads to better thermal resistance. If the gap width is reduced further, thermal resistances better than that of the full-span VGs can be achieved, but there is an optimal gap of around 100 μm below which the thermal resistance increases with decreasing gap. This is to be expected since as the gap width shrinks to zero, the performance should eventually tend to that of the full-span VGs.

The pressure drop behaviour of the central-gap VGs is simpler and as to be expected: decreasing the gap monotonically increases the pressure drop from that of a uniform channel. Interestingly, the pressure drop for the central-gap VGs is somewhat higher than for the end-gap VGs with the same overall gap width. This results in a set of PEC curves with rather different shape – see Fig. 14 and compare with Fig. 4. In most cases the PEC value is quite low and diminishes substantially with Re. Only for relatively large gaps does the PEC value approach unity. For very wide gaps, the PEC value can exceed unity – notably for the C5 VG, which has a single central gap of width 450 μm, and a corresponding PEC index of almost 1.1 for Re = 2300. Indeed this is the highest PEC value obtained from all the geometries examined here.

As Fig. 13 shows, the C5 VG provides a reduction in thermal resistance compared to a uniform channel, and the performance is almost as good as a full-span VG (the C5 thermal resistance is only 2% higher than the full-span value). However, there is a very large difference in the pressure drops associated with these VGs, which of course translates into the large difference in PEC index (1.1 versus 0.7 for C5 and full-span). Clearly, if the thermal resistance of the C5 VG is sufficiently low to maintain the required temperature of the system being cooled, it would appear to be a much preferable choice over the full-span VG as a result of the much lower pumping costs associated with it. This is considered again in section 5.4.4.

13

Though the pressure drop is quite high, the central gap VGs are effective in reducing the local temperature in the solid. To illustrate the temperature reduction that can be achieved relative to the full-span VGs, Fig. 15 compares (on the same scale) the temperature contours on a *y-z* cross-section through the fluid and solid, located just behind the first VG in the channel. Using VGs with a 100 μm central gap, the solid base at this point in the channel is cooled some 12K lower than with full-span VGs. Fig. 15 also indicates the more disturbed flow created by the C-type VG relative to the full-span VG, and the thinner thermal boundary layer. The temperature distributions along the channel are considered later, in section 5.4.

5.3 The effect of combining central and end gaps

Since a central gap and end gaps have each been shown to be beneficial, it is natural to ask if combining them in a single VG would provide even better performance. Fig. 16 shows the calculated thermal resistance of CE-type VGs which have a fixed gap of 100 μm at each end, and a central gap that is varied from 50 to 250 μm. The gap widths indicated in the legend refer to the combined width of all three gaps. The end gaps in these VGs are equivalent to those in the E3 vortex generator (see Table 1). Comparing the E3 curve in Fig. 3 with the curves in Fig. 16 shows that introducing the central gap in addition to the end gaps actually degrades the performance in terms of heat transfer – i.e. the thermal resistance increases. Opening up a central route for the flow reduces the intensity of the flow through the end gaps, and consequently the strength of the longitudinal vortices generated near the channel walls and base. As the central gap is widened, the thermal resistance increases and approaches that of a uniform channel without VGs present.

Thinking in terms of the solid parts of the VGs rather than the gaps, an interesting corollary to the above observation is that two localised short cylindrical VGs are less effective in improving the thermal resistance than two small gaps at the ends of an otherwise solid VG. The PEC index values for the CE-type VGs are all less than unity; they mainly follow a similar profile to Fig. 4, with PEC values between 0.9 and 0.97, apart from the smallest gap (CE1), whose PEC index falls off more sharply with *Re*, reaching a value of 0.88.

5.4 Comparison of the 'best' of each vortex generator type

Having explored separately three different gap configurations, this section compares them against each other. Specifically the 'best' of each type of VG is considered, where 'best' refers to the gap width that provides the lowest thermal resistance for each VG type.

5.4.1 Thermal resistance and pressure drop

As can be seen in Fig. 17, the lowest overall thermal resistance is that of the E2 vortex generators then, in order, the C2, CE1, and full-span VGs, all of which reduce the thermal resistance below that of a uniform channel. The end gaps of the E-type VGs are most effective as the longitudinal vortices are generated close to the side wall, meaning that they can improve the alignment of the flow with the temperature gradient normal to both the channel side wall and the base.

Of these VGs, the lowest pressure drop is that of the CE1 VG, followed in ascending order by E2, the full-span, and finally the C2 VG. Somewhat surprisingly, the C2 VG, with a single central gap of 100 μm, produces a higher pressure drop than the full-span VG. This is attributed to the increased viscous drag from the vertical sides of the narrow gap. For larger central gaps (wider than about 150 μm) the pressure drop is reduced below the level of the full-span VG, as the flow route through the gap opens up. The E2 VG, on the other hand, produces a lower pressure drop than the full-span VG, even though it has two narrow gaps of 75 μm. This is because at the ends of the VG the viscous drag is dominated by the much larger vertical side walls of the channel, and the more open flow path introduced by the gaps quickly outweighs any relatively small additional viscous drag. The CE1 VG has a larger overall gap width, so its low pressure drop is to be expected.

5.4.2 Thermal-hydraulic performance index

Fig. 18 plots the PEC index against Reynolds number for the VGs of each type that produce the greatest thermal conductance (i.e. lowest thermal resistance), and includes for reference the PEC index for the full-span VG system. Clearly the large increase in the pressure drop when full-span VGs are present is not compensated by a commensurate improvement in thermal conductance, and the PEC value is less than 0.8, falling to 0.7 at higher *Re*. Introducing gaps into the VGs improves the PEC index, but the high pressure drop of the C2 VGs means that the PEC value is not much better than the full-span VGs. Although the CE1 VG has a low pressure drop, its relatively poor improvement in the thermal conductance results in PEC values below unity but better than the C2 VG. The best PEC is that of the E2 VG, which, as seen already, has a good PEC index close to unity. This behaviour highlights the fact that the small end gaps promote more intense longitudinal flow disturbances along the length of the channel side wall, enhancing heat transfer from the side wall as well as the base surface.

15

5.4.3 Solid and fluid temperature distributions

For a more visual picture of the performance of the different VGs in terms of the temperature distributions, Fig. 19 shows temperature contours on vertical and horizontal longitudinal cross-sections of the channel for the same VGs as in Fig. 17 operating at Re = 300. For comparison, corresponding contours for the uniform channel (i.e. without VGs) are also included. In the full-span VG plot in Fig. 19 (a) the presence of the closed transverse vortex generated behind each VG (see Fig. 5a) is clearly seen in the elevated temperatures of the fluid there, and there is some localised reduction in the solid temperature as a result (see Fig. 19b). Also shown well in Fig. 19(a), in the 'E2' plot, is the trail of hotter fluid that is transported upwards and into the bulk stream by the longitudinal disturbance generated by the gap between the VG and the channel wall. Compare this with the blue fluid trajectories plotted in Fig. 5(b). This clearly leads to a substantially reduced temperature of the solid base, as can be seen in Fig. 19(b). A similar uplift of warmer fluid behind the VGs is seen in the 'CE1' plot of Fig. 19(a), but the effect is weaker as a result of the central gap diminishing the flow through the end gaps. The flow through the single 100 μm central gaps in the C-type VGs clearly improves the local heat transfer at each VG, as the temperatures of the VGs shows, but there is also a longitudinal effect visible on comparing the 'C2' and full-span plots in Fig. 19, which improves heat transfer to the fluid along the length of the channel downstream of the first VG.

To complement the side- and bottom-view plots of Fig. 19, Fig. 20 shows velocity and temperature plots on spanwise cross-sections of the channel. The velocity contours in Fig. 20(a) show the x-component, with positive values indicating flow towards the outlet and (dark blue) negative values corresponding to reverse flow. The cross-sections are located 100 μm downstream of the first VG (the position indicated approximately by the white dashed line in Fig. 19a), and also show the y-z velocity vectors. The full-span plot shows the strong down-channel flow above the VG and low-velocity flow immediately behind the VG. In contrast, the CE, C and E plots show the enhanced velocity arising from the gaps. The CE gaps are the widest, and this is reflected in the faster flow at the bottom left and the correspondingly reduced speed of the flow over the top of the VG. The swirling effect generated by the gaps in the three cases is also visible in the y-z velocity vectors. As discussed above, the end gaps generate a flow directed upwards along the channel wall, and this is visible in the circulatory patterns in Fig. 20 (indicated by the overlaid arrows). In contrast, when a single central gap is present, the circulation generated is in the opposite sense, leading to a flow down the channel wall.

16

Fig 20(b) shows temperature contours on a cross-section located 2000 μm downstream of the centre of the last VG in the channel, which is the location indicated approximately by the black dashed line in Fig. 19(a). The plots also show *y-z* velocity vectors. The temperature contours clearly show that the E-type VG produces a significantly lower solid temperature than the other VG geometries. The longitudinal vortex created by the gap is also evident in the swirl of the velocity vectors in the rightmost plot of Fig. 20(b), and this allows better penetration of the cooler fluid into the corner between the side wall and base. A similar vortex can be seen in the CE-type VG plot, but the intensity is much reduced by the presence of the additional flow route through the central gap. For the C-type VG, a substantial central plume of warmer fluid can be seen as a result of the single central gap promoting heat transfer from the base of the channel. However, the C-type and CE-type VGs both exhibit thicker thermal boundary layers in this region downstream of the final VG, resulting in slightly higher solid temperatures here than for the full-span VG, despite the temperatures upstream being lower than for the full-span VG. This will be considered further in section 5.4.4.

5.4.4 Base surface temperatures

In the practical application of a microchannel heat sink (e.g. in cooling a microprocessor chip, as was the motivation for the present study), a vital quantity of interest is the actual surface temperature that can be achieved with a given microchannel geometry, under a given heat load. Therefore, as a final observation, Fig. 21 presents the average and, importantly, maximum temperatures achieved on the bottom surface of the heat sink operating at *Re* = 1500 with channels containing the C, E and CE-type VGs offering the lowest thermal resistance. Recall that the heat flux entering the solid base from below is 100 W/cm^2, and the inlet fluid temperature is 293.15 K. Also included for comparison is the corresponding data for a uniform channel with no VGs, a channel with full-span VGs, and a channel with C5 VGs (which have the highest PEC index of 1.08 at this Reynolds number).

First, it can be seen that the channels with vortex generators all produce a lower average temperature than the uniform channel, as has already been seen through the thermal resistance, equation (6), which is based on the average temperature. However, the maximum temperatures obtained (at the outflow) show a rather different behaviour. The full-span VG provides a 2 K reduction in the average surface temperature and a 2.5 K reduction in the maximum temperature compared to the uniform channel. Introducing the end gaps to create the E2 VGs produces a further 4 K reduction in the average and 1.6 K reduction in the maximum temperature, and is clearly beneficial. However, the C-type and CE-type VGs do

17

not significantly reduce the maximum temperature relative to the uniform channel – in fact the CE1 VG actually results in an almost 1 K *increase* in the maximum temperature. Similarly the C5 VG offers no reduction in the maximum temperature compared to the uniform channel, despite providing a similar thermal resistance and hence average surface temperature to the full-span VG, as remarked above. This suggests that the improvements in heat transfer offered by the C-type and CE-type VGs are somewhat more localised, such that over the whole surface the net effect is a reduction in average temperature, but at the expense of other areas where the local heat transfer is worse. Indeed, this effect can be seen at the left-most ends of the contour plots in Fig. 19, where the C2 and CE1 VGs have a thicker thermal boundary layer on the base surface than the other VG types.

The temperature plots in Fig. 19 suggest that the E-type and full-span VGs are essentially independent of each other at this spacing between the VGs; the transverse vortices generated by the full-span VGs do not extend as far as the next VG, and for the E-type VG, the fluid passing through the gaps is swept upwards and inwards away from the gaps in the next VG. In contrast, the C2 and CE1 VGs show more interaction, with a more closed region of higher temperature fluid between consecutive VGs. Hence for the C2 and CE1 VGs, the flow downstream of the final VG is more different from the upstream flow than in the E-type and full-span cases. This indicates that placement and distribution of the VGs within the channel is an important additional design factor for consideration, but this is beyond the scope of the present study.

The base surface temperature results highlight that, although the PEC can be useful in comparing designs, it does not provide a complete picture of performance in terms of the practical objective maintaining temperature below a given threshold. The results of Fig. 21 do however show further evidence that having gaps between the ends of the VGs and channel walls is beneficial.

6. Conclusions

The 3D numerical analysis presented here set out to examine the benefits of having various gaps along the span of cylindrical vortex generators placed across the base of a water-filled micro-channel to enhance heat transfer. The geometries have been assessed at Reynolds number 300-2300 in terms of their thermal resistances, pressure drops, a performance evaluation criteria index combining both of these, and the maximum temperature of the

18

base. The baseline geometry is a micro-channel containing solid full-span VGs, which generate transverse vortices.

It was found that, by all measures, having gaps between each end of the VGs and the channel side walls offers enhanced performance. Introducing these gaps produces longitudinal vortices adjacent to the channel side walls which enhance the heat transfer from those walls into the bulk flow. Importantly, three-dimensional tracer particle trajectory plots show that in addition to the longitudinal vortices generated downstream of the VGs, the fluid passing through the end gap is swept upwards and inwards, where it remains as it flows onwards to the outflow. This provides a significant additional heat transfer route for hot fluid to be transported directly away from the solid surfaces. The presence of the end gaps also reduces the pressure drop compared to the full-span VG, and for gaps of 100 µm at each end the PEC index is slightly above one for most Reynolds numbers, indicating that the pressure drop penalty compared to a uniform channel is more than compensated for by the improvement in thermal conductivity. The gap size offering the best thermal conductivity, and the lowest maximum base temperature, is 75 µm at each end, for which the PEC index is close to 1, i.e. neutral, especially at higher *Re*.

Having a single central gap was found to offer localised enhancement of heat transfer, which when considered over the whole base surface produced a lower average temperature and hence lower thermal resistance. However, the maximum temperature of the base, close to the outflow, is actually higher than that for a full-span VG, and close to that for a uniform channel without VGs present. From a practical perspective of maintaining the base of the heat sink at a given temperature, this is clearly undesirable. Small central gaps (e.g. 100 µm) are also found to increase the pressure drop relative to the full-span VG, and the PEC index for such gap sizes is correspondingly poor. On the other hand, large central gaps (e.g. 450 µm) have a high PEC index of up to 1.1, but produce average temperatures slightly above those for the full-span VG and maximum temperatures above even those for a uniform channel. This highlights that the PEC index should only be used in conjunction with specific actual rather than relative measurements of performance. Combining a central gap together with end gaps (of 100 µm) was found not to be beneficial, as the negative aspects of the central gap generally outweighed the positive effects of the end gaps.

There are of course many other configurations of VG gaps that could be considered for analysis, such as gaps that are staggered between consecutive VGs, rather than aligned as in the present study, and different spacing and distributions of the VGs within the channel. However, the clear conclusion from this work is that gaps at the ends of the VGs are beneficial in terms of the average and maximum temperatures that can be achieved for a given heat load, and in reducing the large pressure drop associated with full-span cylindrical

19

vortex generators. The end-gap configuration outperforms the other configurations explored here, but there is an optimum end-gap width below which the pressure drop increases rapidly with no gain in heat transfer performance. For the system considered here, this gap was found to be 15% of the channel width.

References

[1] H.-Y. Li, C.-L. Chen, S.-M. Chao, and G.-F. Liang, "Enhancing heat transfer in a plate-fin heat sink using delta winglet vortex generators," *International Journal of Heat and Mass Transfer,* vol. 67, pp. 666-677, 12/ 2013.

[2] Y. F. Li, G. D. Xia, D. D. Ma, Y. T. Jia, and J. Wang, "Characteristics of laminar flow and heat transfer in microchannel heat sink with triangular cavities and rectangular ribs," *International Journal of Heat and Mass Transfer,* vol. 98, pp. 17-28, 7// 2016.

[3] H. Alipour, A. Karimipour, M. R. Safaei, D. T. Semiromi, and O. A. Akbari, "Influence of T-semi attached rib on turbulent flow and heat transfer parameters of a silver-water nanofluid with different volume fractions in a three-dimensional trapezoidal microchannel," *Physica E: Low-dimensional Systems and Nanostructures,* vol. 88, pp. 60-76, 4/ 2017.

[4] M. T. Al-asadi, H. A. Mohammed, A. S. Kherbeet, and A. A. Al-aswadi, "Numerical study of assisting and opposing mixed convective nanofluid flows in an inclined circular pipe," *International Communications in Heat and Mass Transfer,* vol. 85, pp. 81-91, 7// 2017.

[5] J. Albadr, S. Tayal, and M. Alasadi, "Heat transfer through heat exchanger using Al_2O_3 nanofluid at different concentrations," *Case Studies in Thermal Engineering,* vol. 1, pp. 38-44, 10/1/ 2013.

[6] M. Cheraghi, M. Raisee, and M. Moghaddami, "Effect of cylinder proximity to the wall on channel flow heat transfer enhancement," *Comptes Rendus Mécanique,* vol. 342, pp. 63-72, 2/ 2014.

[7] M. R. Safaei, A. Jahanbin, A. Kianifar, S. Gharehkhani, A. S. Kherbeet, M. Goodarzi*, et al.*, "Mathematical Modeling for Nanofluids Simulation: A Review of the Latest Works," in *Modeling and Simulation in Engineering Sciences*, N. S. Akbar and O. A. Beg, Eds., ed Rijeka: InTech, 2016, p. Ch. 09.

[8] A. S. Kherbeet, H. A. Mohammed, H. E. Ahmed, B. H. Salman, O. A. Alawi, M. R. Safaei*, et al.*, "Mixed convection nanofluid flow over microscale forward-facing step — Effect of inclination and step heights," *International Communications in Heat and Mass Transfer,* vol. 78, pp. 145-154, 11/ 2016.

[9] A. Koşar, "Effect of substrate thickness and material on heat transfer in microchannel heat sinks," *International Journal of Thermal Sciences,* vol. 49, pp. 635-642, 2010/04/01/ 2010.

[10] T. Dixit and I. Ghosh, "Review of micro- and mini-channel heat sinks and heat exchangers for single phase fluids," *Renewable and Sustainable Energy Reviews,* vol. 41, pp. 1298-1311, 1/ 2015.

[11] S. S. Mehendale, A. M. Jacobi, and R. K. Shah, "Fluid Flow and Heat Transfer at Micro- and Meso-Scales With Application to Heat Exchanger Design," *Applied Mechanics Reviews,* vol. 53, pp. 175-193, 2000.

[12] G. W. Kandlikar SG, "Evolution of microchannel flow passages: thermohydraulic performance and fabrication technology.," *Proceedings of the ASME international mechanical engineering congress exposition,* 2002.

[13] D. B. Tuckerman and R. F. W. Pease, "High-performance heat sinking for VLSI," *Electron Device Letters, IEEE,* vol. 2, pp. 126-129, 1981.

[14] C. Nonino, S. Savino, S. Del Giudice, and L. Mansutti, "Conjugate forced convection and heat conduction in circular microchannels," *International Journal of Heat and Fluid Flow,* vol. 30, pp. 823-830, 2009/10/01/ 2009.

[15] D. C. Knupp, R. M. Cotta, and C. P. Naveira-Cotta, "Heat Transfer in Microchannels with Upstream–Downstream Regions Coupling and Wall Conjugation Effects," *Numerical Heat Transfer, Part B: Fundamentals,* vol. 64, pp. 365-387, 2013/11/01 2013.

[16] G. Gamrat, M. Favre-Marinet, and D. Asendrych, "Conduction and entrance effects on laminar liquid flow and heat transfer in rectangular microchannels," *International Journal of Heat and Mass Transfer,* vol. 48, pp. 2943-2954, 2005/07/01/ 2005.

[17] F. J. Hong, P. Cheng, H. Ge, and G. T. Joo, "Conjugate heat transfer in fractal-shaped microchannel network heat sink for integrated microelectronic cooling application," *International Journal of Heat and Mass Transfer,* vol. 50, pp. 4986-4998, 2007/12/01/ 2007.

[18] O. Manca, S. Nardini, and D. Ricci, "A numerical study of nanofluid forced convection in ribbed channels," *Applied Thermal Engineering,* vol. 37, pp. 280-292, 5/ 2012.

[19] M. A. Ahmed, M. Z. Yusoff, K. C. Ng, and N. H. Shuaib, "Effect of corrugation profile on the thermal–hydraulic performance of corrugated channels using CuO–water nanofluid," *Case Studies in Thermal Engineering,* vol. 4, pp. 65-75, 11/ 2014.

[20] C.-C. Wang and J.-S. Liaw, "Air-side performance of herringbone wavy fin-and-tube heat exchangers under dehumidifying condition – Data with larger diameter tube," *International Journal of Heat and Mass Transfer,* vol. 55, pp. 3054-3060, 5/ 2012.

[21] L. Li, X. Du, Y. Zhang, L. Yang, and Y. Yang, "Numerical simulation on flow and heat transfer of fin-and-tube heat exchanger with longitudinal vortex generators," *International Journal of Thermal Sciences,* vol. 92, pp. 85-96, 6/ 2015.

[22] J. M. Wu and W. Q. Tao, "Numerical study on laminar convection heat transfer in a rectangular channel with longitudinal vortex generator. Part A: Verification of field synergy principle," *International Journal of Heat and Mass Transfer,* vol. 51, pp. 1179-1191, 3/ 2008.

[23] C.-C. Wang, J. Lo, Y.-T. Lin, and M.-S. Liu, "Flow visualization of wave-type vortex generators having inline fin-tube arrangement," *International Journal of Heat and Mass Transfer,* vol. 45, pp. 1933-1944, 4/ 2002.

[24] T. Johnson and P. Joubert, "The influence of vortex generators on the drag and heat transfer from a circular cylinder normal to an airstream," *Journal of Heat Transfer,* vol. 91, pp. 91-99, 1969.

[25] A. Ebrahimi, E. Roohi, and S. Kheradmand, "Numerical study of liquid flow and heat transfer in rectangular microchannel with longitudinal vortex generators," *Applied Thermal Engineering,* vol. 78, pp. 576-583, 3/5/ 2015.

[26] H. E. Ahmed, H. A. Mohammed, and M. Z. Yusoff, "An overview on heat transfer augmentation using vortex generators and nanofluids: Approaches and applications," *Renewable and Sustainable Energy Reviews,* vol. 16, pp. 5951-5993, 10/ 2012.

[27] A. Behnampour, O. A. Akbari, M. R. Safaei, M. Ghavami, A. Marzban, G. A. Sheikh Shabani*, et al.*, "Analysis of heat transfer and nanofluid fluid flow in microchannels with trapezoidal, rectangular and triangular shaped ribs," *Physica E: Low-dimensional Systems and Nanostructures,* vol. 91, pp. 15-31, 7/ 2017.

[28] M. R. Safaei, M. Gooarzi, O. A. Akbari, M. S. Shadloo, and M. Dahari, "Performance Evaluation of Nanofluids in an Inclined Ribbed Microchannel for Electronic Cooling Applications," in *Electronics Cooling*, S. M. S. Murshed, Ed., ed Rijeka: InTech, 2016, p. Ch. 06.

[29] C. Min, C. Qi, X. Kong, and J. Dong, "Experimental study of rectangular channel with modified rectangular longitudinal vortex generators," *International Journal of Heat and Mass Transfer,* vol. 53, pp. 3023-3029, 7/ 2010.

[30] C. Habchi, S. Russeil, D. Bougeard, J.-L. Harion, T. Lemenand, D. Della Valle*, et al.*, "Enhancing heat transfer in vortex generator-type multifunctional heat exchangers," *Applied Thermal Engineering,* vol. 38, pp. 14-25, 5/ 2012.

[31] M. T. Al-Asadi, H. A. M., A. Sh. Kherbeet, and H. K. Dawood, "Heat Transfer Enhancements Using Traditional Fluids and Nanofluids in Pipes with Different Orientations: A Review," *Journal of Nanofluids,* vol. 6, pp. 1-21, 2017.

[32] Y. Kai-Shing, J. Jhih-Hao, L. Yur-Tsai, C. Kuo-Hsiang, and W. Chi-Chuan, "On the Heat Transfer Characteristics of Heat Sinks: With and Without Vortex Generators," *Components and Packaging Technologies, IEEE Transactions on,* vol. 33, pp. 391-397, 2010.

[33] J.-S. Leu, Y.-H. Wu, and J.-Y. Jang, "Heat transfer and fluid flow analysis in plate-fin and tube heat exchangers with a pair of block shape vortex generators," *International Journal of Heat and Mass Transfer,* vol. 47, pp. 4327-4338, 9/ 2004.

[34] J. M. Wu and W. Q. Tao, "Effect of longitudinal vortex generator on heat transfer in rectangular channels," *Applied Thermal Engineering,* vol. 37, pp. 67-72, 5/ 2012.

[35] M. Khoshvaght-Aliabadi, S. Zangouei, and F. Hormozi, "Performance of a plate-fin heat exchanger with vortex-generator channels: 3D-CFD simulation and experimental validation," *International Journal of Thermal Sciences,* vol. 88, pp. 180-192, 2// 2015.

[36] J. Li, S. Wang, J. Chen, and Y.-G. Lei, "Numerical study on a slit fin-and-tube heat exchanger with longitudinal vortex generators," *International Journal of Heat and Mass Transfer,* vol. 54, pp. 1743-1751, 4/ 2011.

[37] S. Chomdee and T. Kiatsiriroat, "Enhancement of air cooling in staggered array of electronic modules by integrating delta winglet vortex generators," *International Communications in Heat and Mass Transfer,* vol. 33, pp. 618-626, 5/ 2006.

[38] C. Liu, J.-t. Teng, J.-C. Chu, Y.-l. Chiu, S. Huang, S. Jin*, et al.*, "Experimental investigations on liquid flow and heat transfer in rectangular microchannel with longitudinal vortex generators," *International Journal of Heat and Mass Transfer,* vol. 54, pp. 3069-3080, 6/ 2011.

[39] J. Ma, Y. P. Huang, J. Huang, Y. L. Wang, and Q. W. Wang, "Experimental investigations on single-phase heat transfer enhancement with longitudinal vortices in narrow rectangular channel," *Nuclear Engineering and Design,* vol. 240, pp. 92-102, 1/ 2010.

[40] G. D. Xia, J. Jiang, J. Wang, Y. L. Zhai, and D. D. Ma, "Effects of different geometric structures on fluid flow and heat transfer performance in microchannel heat sinks," *International Journal of Heat and Mass Transfer,* vol. 80, pp. 439-447, 1/ 2015.

[41] C. Chen, J.-T. Teng, C.-H. Cheng, S. Jin, S. Huang, C. Liu*, et al.*, "A study on fluid flow and heat transfer in rectangular microchannels with various longitudinal vortex generators," *International Journal of Heat and Mass Transfer,* vol. 69, pp. 203-214, 2/ 2014.

[42] H. Mirzaee, A. Dadvand, I. Mirzaee, and R. Shabani, "Heat transfer enhancement in microchannels using an elastic vortex generator," *Journal of Enhanced Heat Transfer,* vol. 19, 2012.

[43] J. Wang and Y. Zhao, "Heat and fluid flow characteristics of a rectangular channel with a small diameter circular cylinder as vortex generator," *International Journal of Thermal Sciences,* vol. 92, pp. 1-13, 6/ 2015.

[44] L. Chai, G. D. Xia, and H. S. Wang, "Numerical study of laminar flow and heat transfer in microchannel heat sink with offset ribs on sidewalls," *Applied Thermal Engineering,* vol. 92, pp. 32-41, 2016/01/05/ 2016.

[45] L. Chai, G. D. Xia, and H. S. Wang, "Parametric study on thermal and hydraulic characteristics of laminar flow in microchannel heat sink with fan-shaped ribs on sidewalls – Part 1: Heat transfer," *International Journal of Heat and Mass Transfer,* vol. 97, pp. 1069-1080, 2016/06/01/ 2016.

[46] L. Chai, G. D. Xia, and H. S. Wang, "Parametric study on thermal and hydraulic characteristics of laminar flow in microchannel heat sink with fan-

shaped ribs on sidewalls – Part 2: Pressure drop," *International Journal of Heat and Mass Transfer,* vol. 97, pp. 1081-1090, 2016/06/01/ 2016.

[47]   L. Chai, G. D. Xia, and H. S. Wang, "Parametric study on thermal and hydraulic characteristics of laminar flow in microchannel heat sink with fan-shaped ribs on sidewalls – Part 3: Performance evaluation," *International Journal of Heat and Mass Transfer,* vol. 97, pp. 1091-1101, 2016/06/01/ 2016.

[48]   M. T. Al-Asadi, F. S. Alkasmoul, and M. C. T. Wilson, "Heat transfer enhancement in a micro-channel cooling system using cylindrical vortex generators," *International Communications in Heat and Mass Transfer,* vol. 74, pp. 40-47, 5/ 2016.

[49]   K. Kawano, K. Minakami, H. Iwasaki, and M. Ishizuka, "Micro channel heat exchanger for cooling electrical equipment," *ASME Heat Transfer Div Publ Htd,* vol. 361, pp. 173-180, 1998.

[50]   W. Qu and I. Mudawar, "Analysis of three-dimensional heat transfer in micro-channel heat sinks," *International Journal of Heat and Mass Transfer,* vol. 45, pp. 3973-3985, 09/01/ 2002.

[51]   X. Yu, J. Feng, Q. Feng, and Q. Wang, "Development of a plate-pin fin heat sink and its performance comparisons with a plate fin heat sink," *Applied Thermal Engineering,* vol. 25, pp. 173-182, 2/ 2005.

[52]   S. P. Gurrum, S. K. Suman, Y. K. Joshi, and A. G. Fedorov, "Thermal issues in next-generation integrated circuits," *Device and Materials Reliability, IEEE Transactions on,* vol. 4, pp. 709-714, 2004.

[53]   W. Yuan, J. Zhao, C. P. Tso, T. Wu, W. Liu, and T. Ming, "Numerical simulation of the thermal hydraulic performance of a plate pin fin heat sink," *Applied Thermal Engineering,* vol. 48, pp. 81-88, 12/15/ 2012.

Table captions

24

Table 1: Dimensions of the micro-channel and VG configurations considered. The gap dimensions refer to the overall combined gap size. For the E-type VGs, this is made up of two equal-width gaps, one at each end. For the CE-type VGs, the gaps at the ends are fixed at 100 µm each, and the size of the central gap is varied.

Micro- channel dimensions, µm					
L	25000	H_b	200	H_c	700
W_w	300	W_c	500	r	0-500

Gap dimensions, µm					
Central gap (C)		End gap (E)		Central and End gaps (CE)	
C1	50	E1	50	CE1	250
C2	100	E2	150	CE2	300
C3	150	E3	200	CE3	350
C4	400	E4	250	CE4	400
C5	450	E5	300	CE5	450
		E6	350		
		E7	400		

Table 2: Boundary conditions. Note that $\boldsymbol{n}$ represents the normal to the boundary

Position	Condition	Equations
Right and left outer walls	symmetry	$\frac{\partial T_L}{\partial y} = \frac{\partial T_S}{\partial y} = \frac{\partial u}{\partial y} = \frac{\partial w}{\partial y} = v = 0$
Bottom wall	uniform heat flux, q	$-k_S \frac{\partial T_S}{\partial z} = q$
Fluid inlet, $x = x_{in}$	uniform velocity	$\boldsymbol{u}(x_{in}, y, z) = (u_{in}, 0,0) = (\frac{\mu Re}{\rho D_h}, 0,0)$
Fluid outlet	pressure	$p = 0$
Fluid-solid interface	continuity of temperature and flux; no slip	$T_S = T_L, \boldsymbol{n} \cdot (k_S \nabla T_S) = \boldsymbol{n} \cdot (k \nabla T_L),$ $\boldsymbol{u} = \boldsymbol{0}$
All other walls	adiabatic	$-\boldsymbol{n} \cdot (k \nabla T) = 0$

Figure captions

25
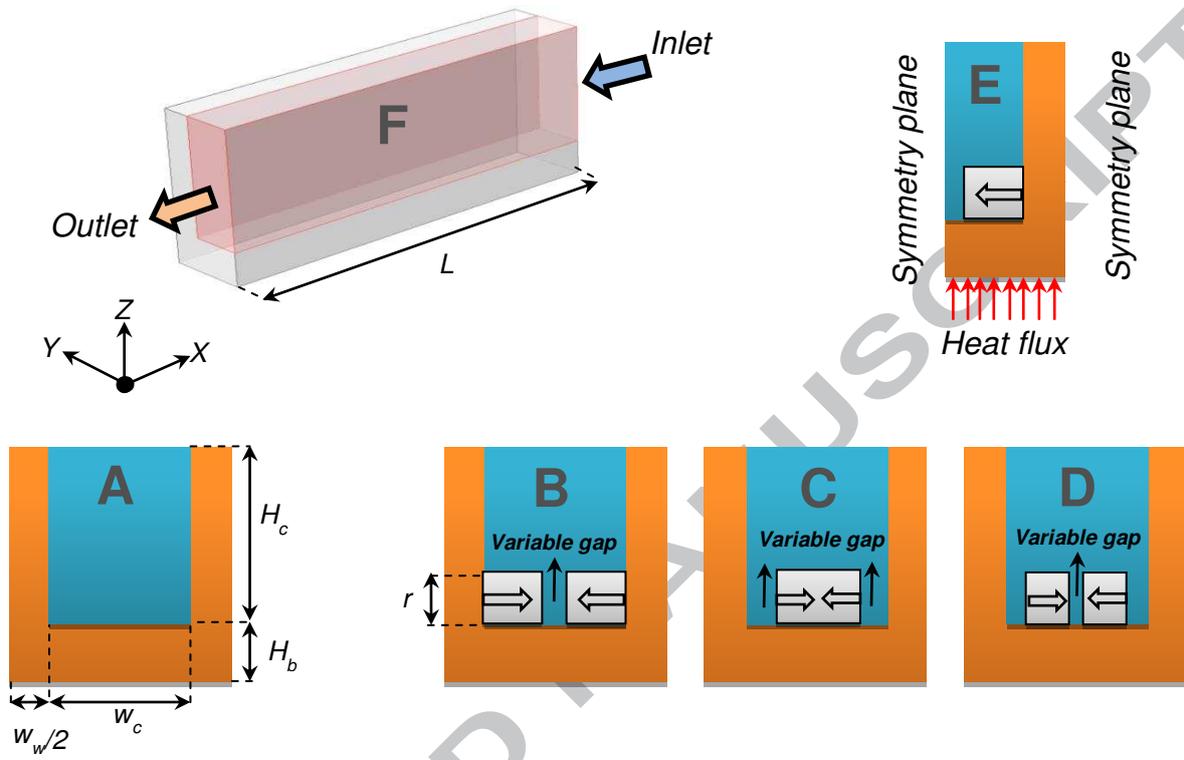
Figure 1: Geometry description: (a) uniform rectangular micro-channel with governing the dimensions of the geometry; (b) front-view cross-section of a 'central' ('C') gap VG; (c) front-view cross-section of an 'end' ('E') gap VG; (d) front-view cross-section of a 'CE' VG, with central and end gaps; (e) boundary conditions applied; (f) 3D view of the uniform channel.
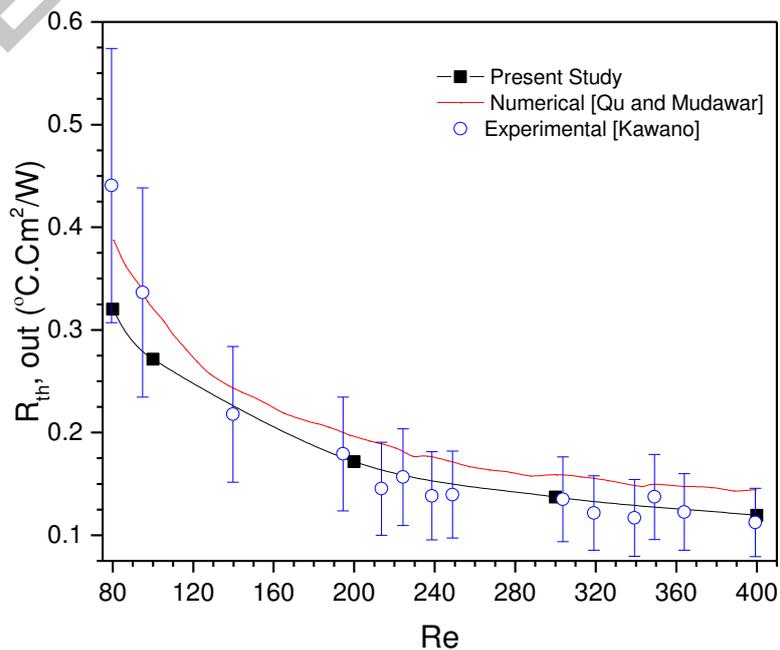
Figure 2: Validation of the present model: thermal resistance in a straight micro-channel results compared with experimental measurements by Kawano et al. [49] and numerical calculations by Qu and Mudawar [50].
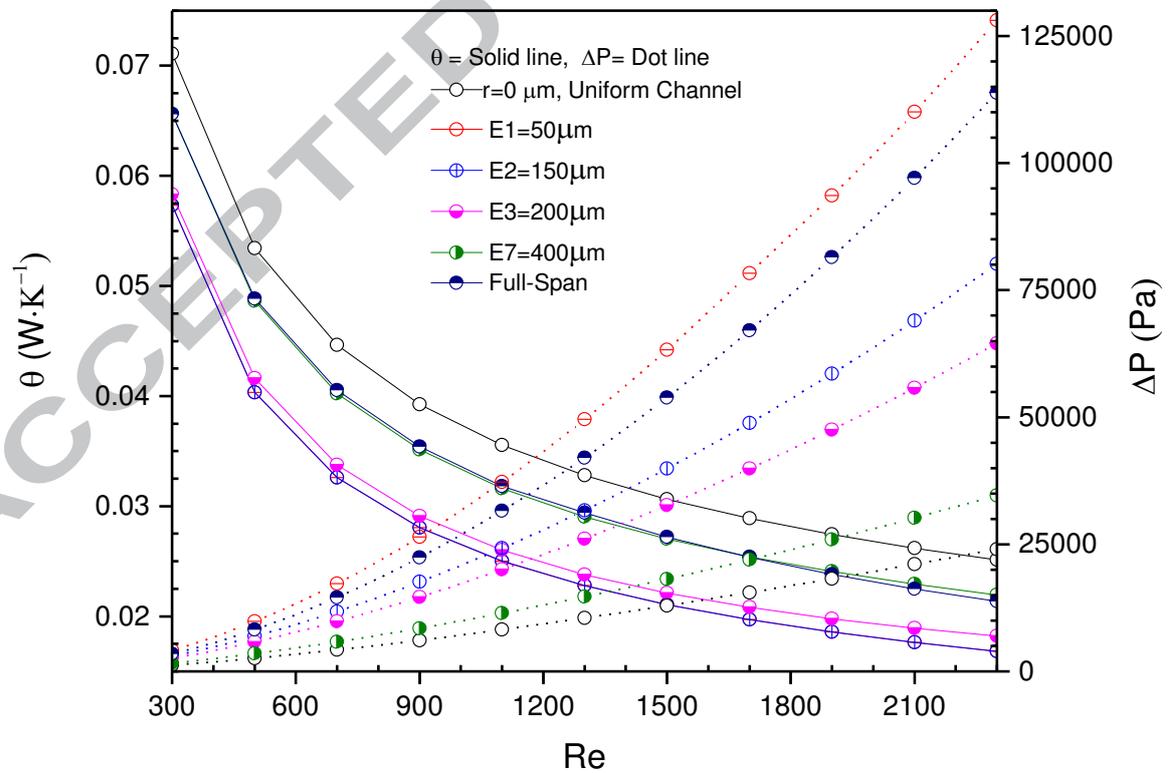
Figure 3: Thermal resistance and pressure drop versus *Re* for E-type VGs of radius 400 µm having various gaps of combined width indicated in the legend. The r = 0 µm line refers to the uniform channel with no VG present.

27
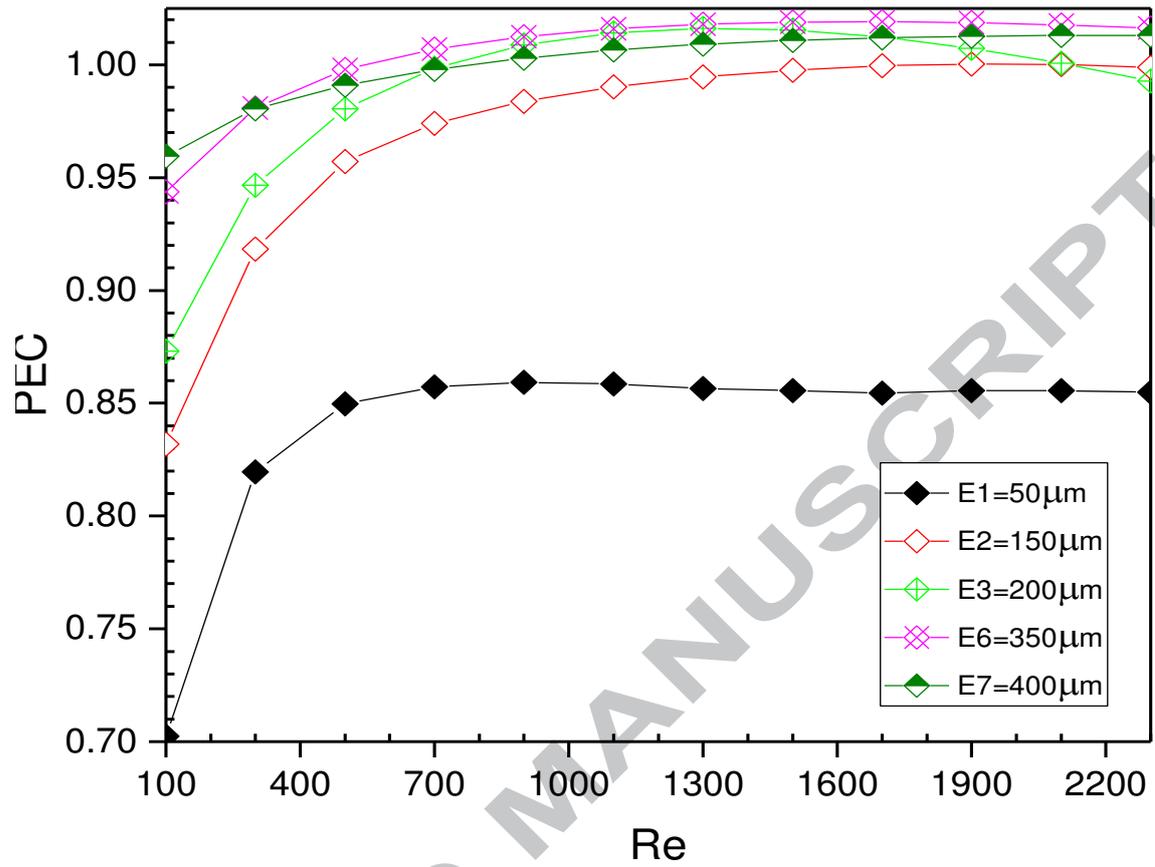
Figure 4: PEC index values for various end-gap widths.

(a)

(b)

(c)

flow is upwards and
away from channel wall
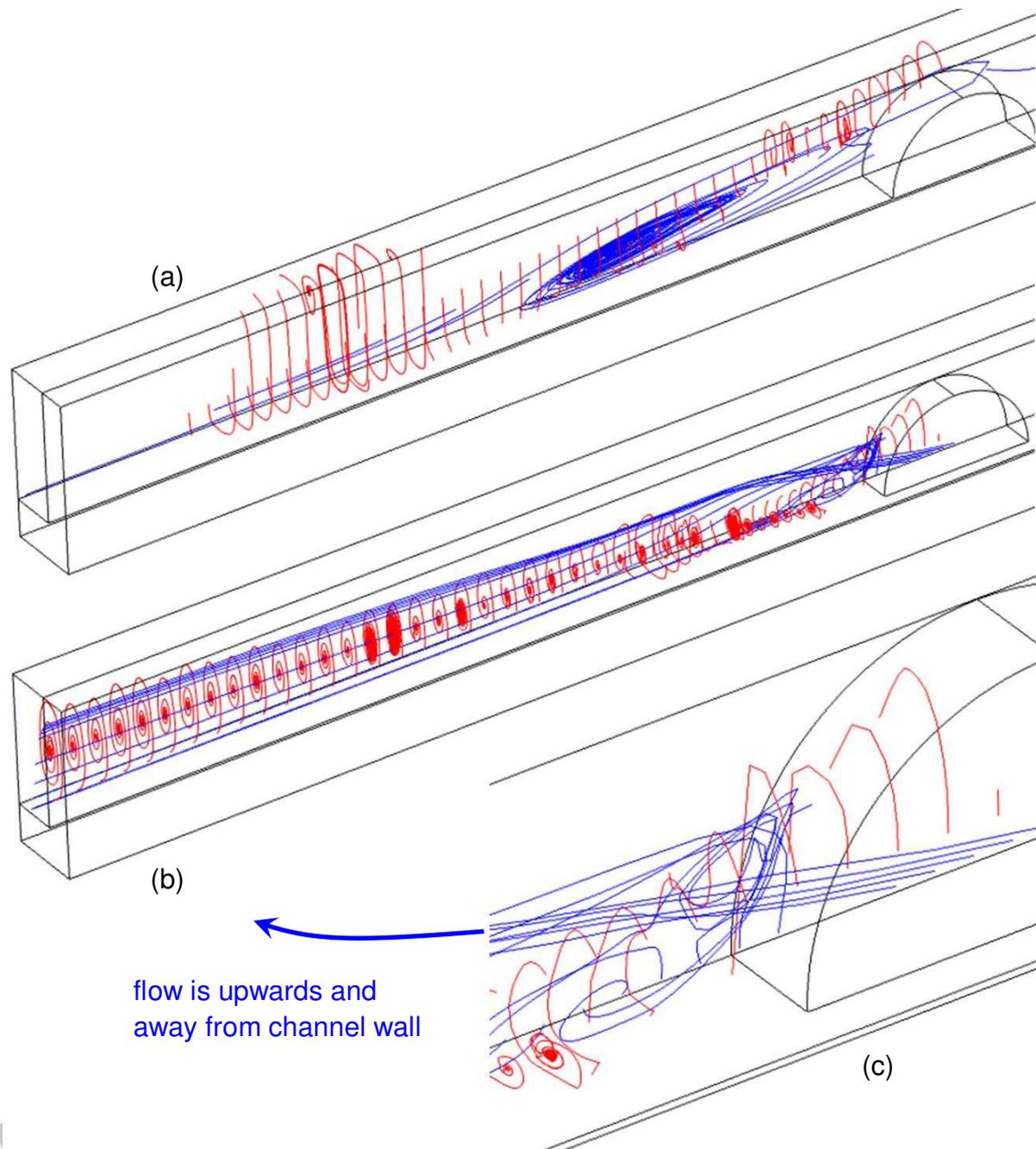
Figure 5: Paths of passive tracer particles in the flow, illustrating the effect of (a) a full-span cylindrical VG and (b) an E-type VG on transverse and longitudinal vortex generation. The VGs have radius 400 μm. The flow is from right to left with Reynolds number 500 and the gap at each end of the VG is 75 μm. Plot (c) is an enlarged view of (b).
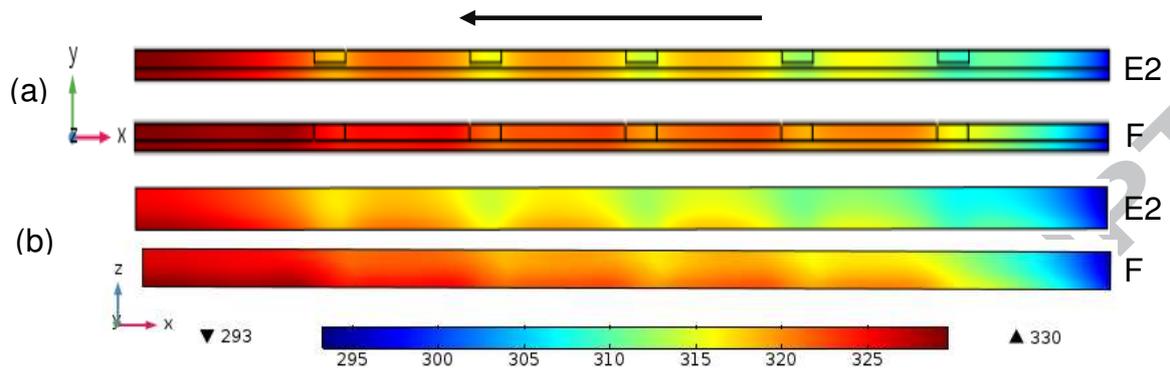
Figure 6: Temperature contours (in K) along channels containing five E2 or full-span (F) VGs. The planes shown are within the solid and located 2 µm away from the water: (a) the base of the channel, (b) the side wall of the channel.
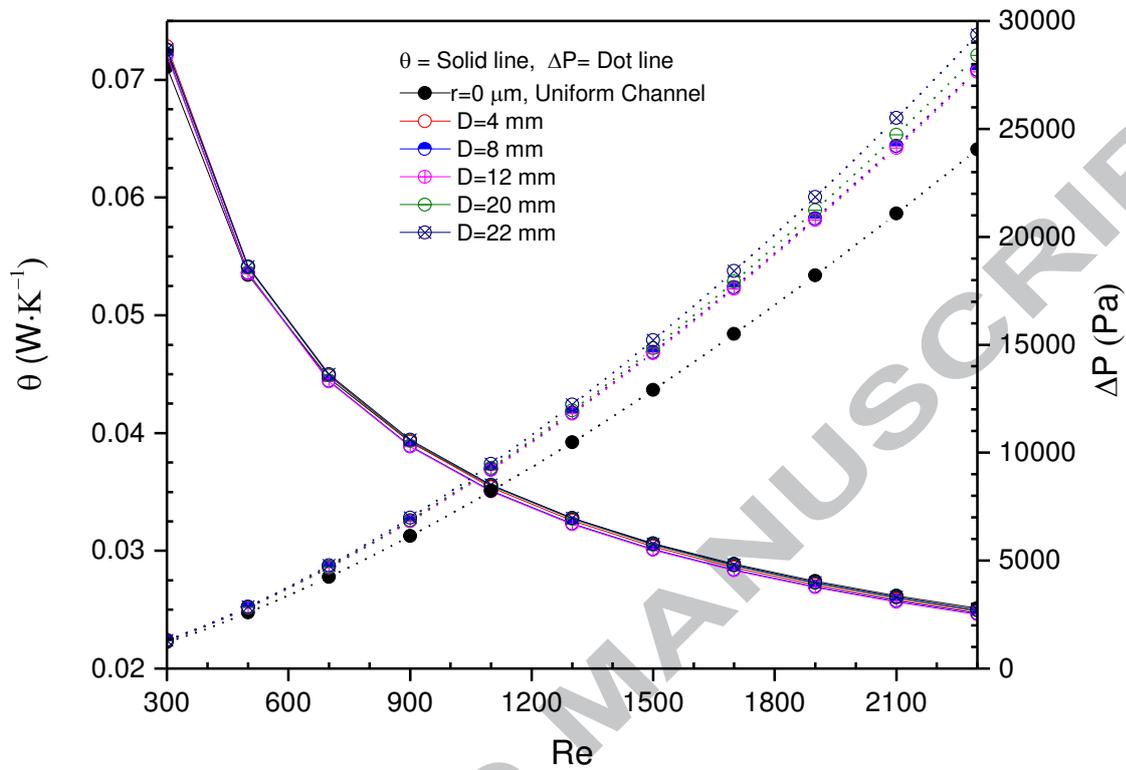
Figure 7: Effect of single E2 VG position on thermal resistance and pressure drop.
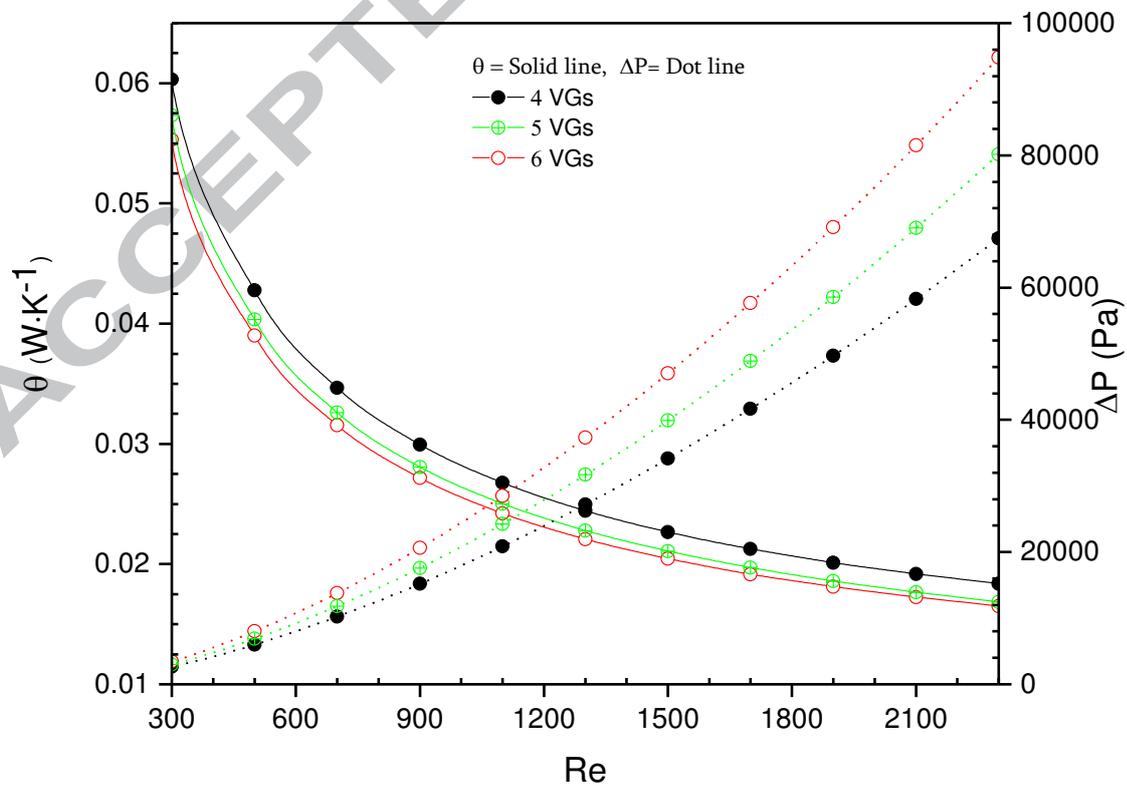
Figure 8: Effect of the number of E2 VGs on thermal resistance and pressure drop.

31
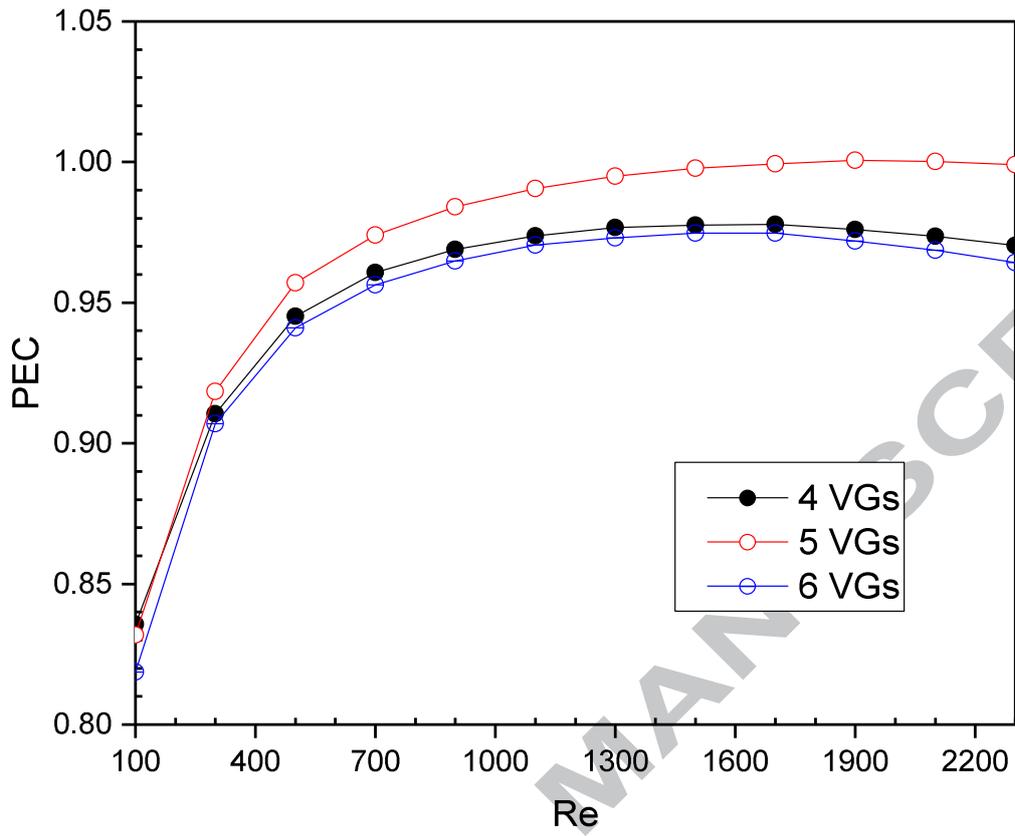
Figure 9: PEC versus *Re* for series of equally-spaced E2 VGs of radius 400 μm.
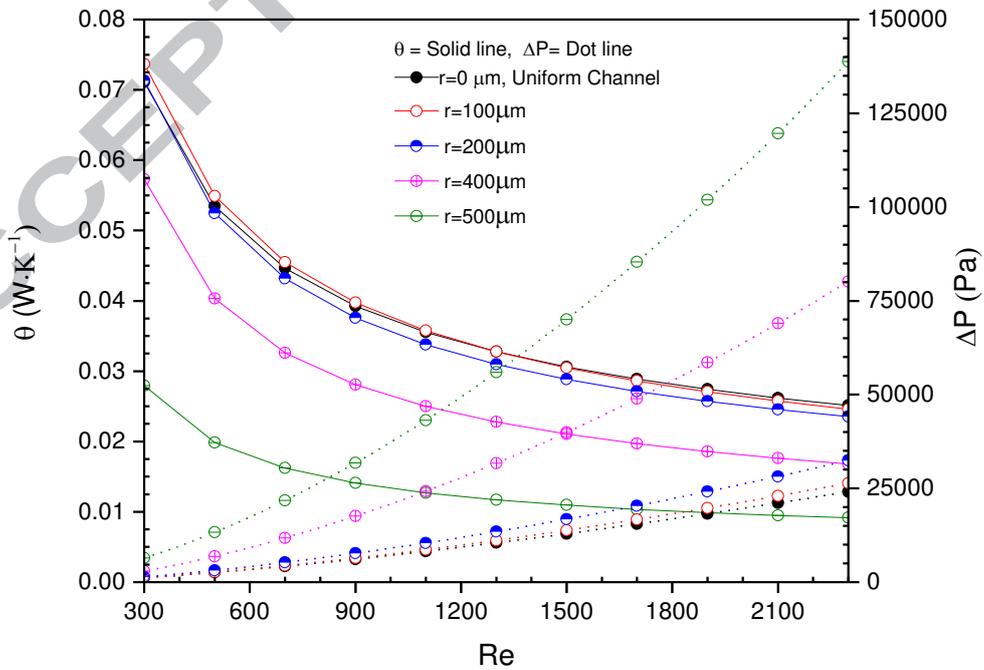
Figure 10: Effect of VG radius on thermal resistance and pressure drop for E2 VGs.
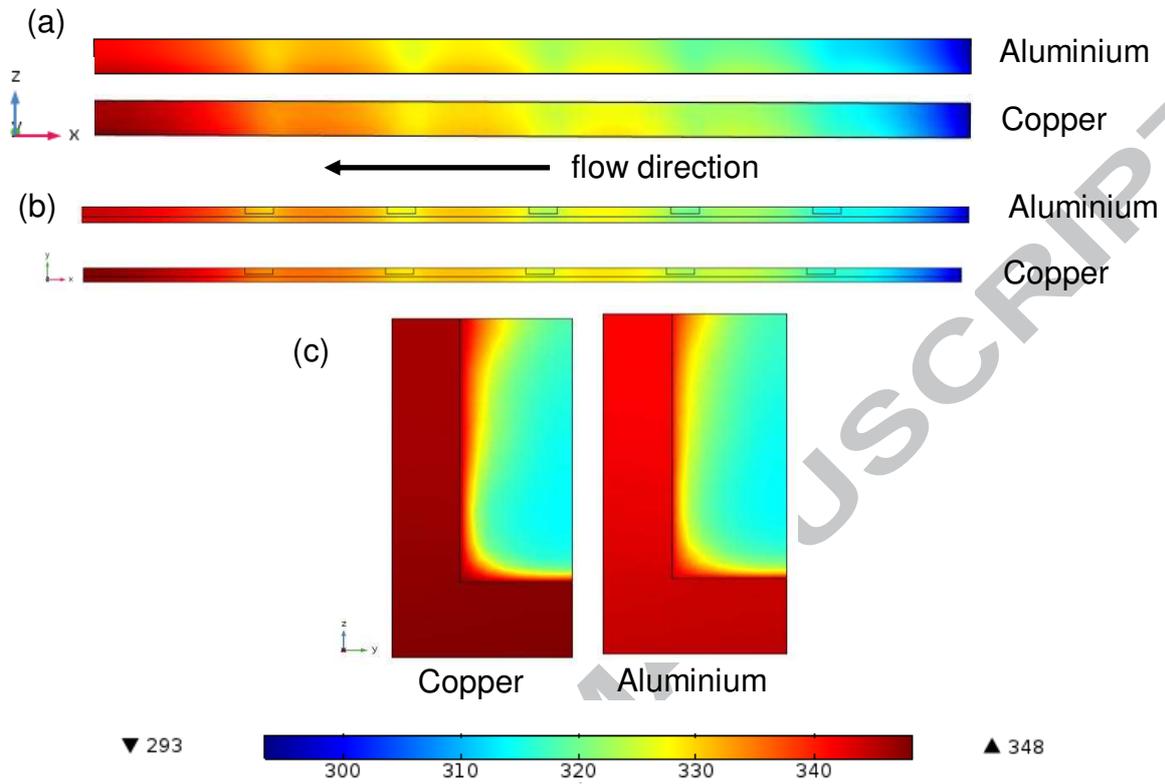
Figure 11: Temperature contours (in K) along copper and aluminium channels containing five E2 VGs of radius 400 µm with flow at Re=300. The planes in (a) and (b) are within the solid, 2 µm away from the water: (a) the side wall of the channel, (b) the base of the channel. The (y,z) cross-sections in (c) are at the outflow.

33
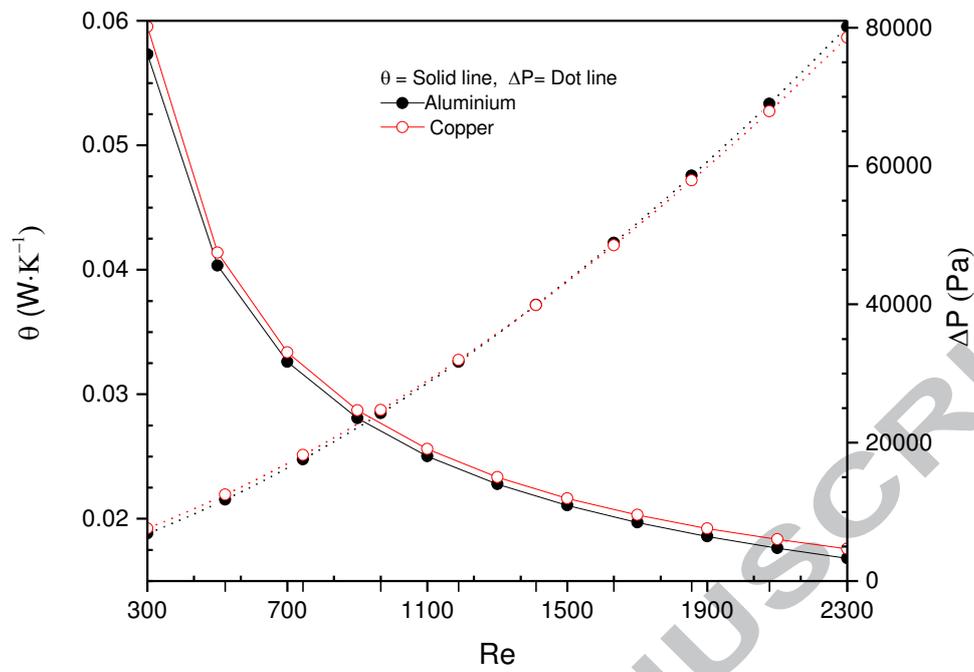
Figure 12: Performance of copper versus aluminium in terms of thermal resistance and pressure drop.
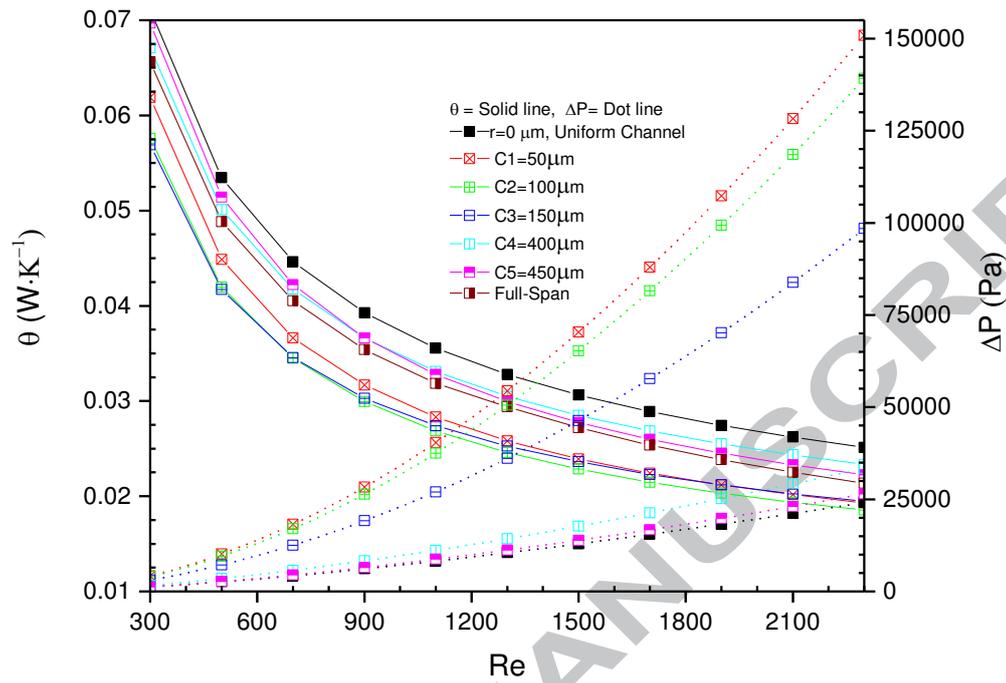
Figure 13: Thermal resistance and pressure drop calculated for C-type cylindrical VGs as a function of Reynolds number.
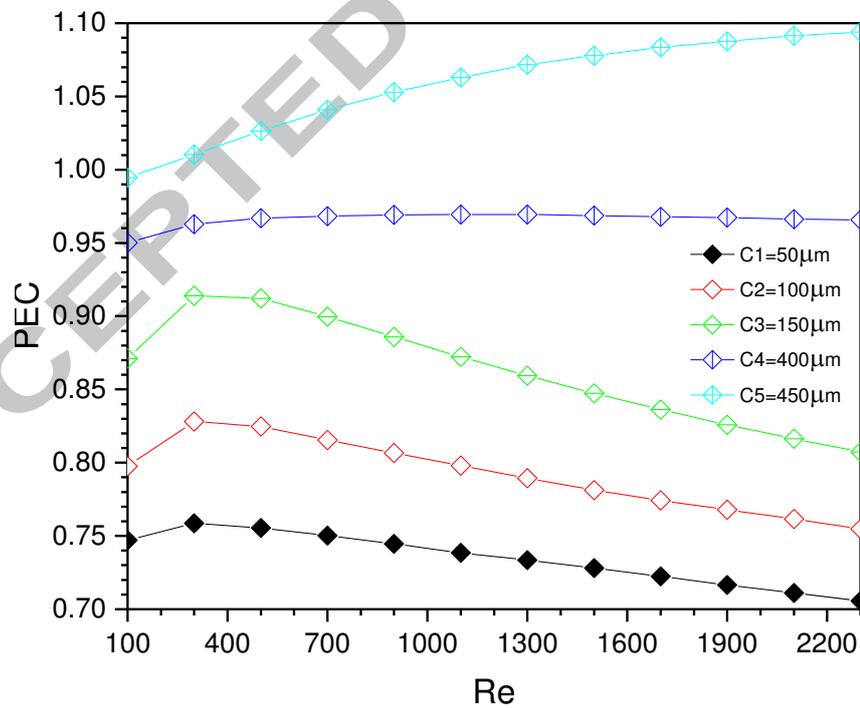
Figure 14: PEC values as a function of Reynolds number for the C-type VGs
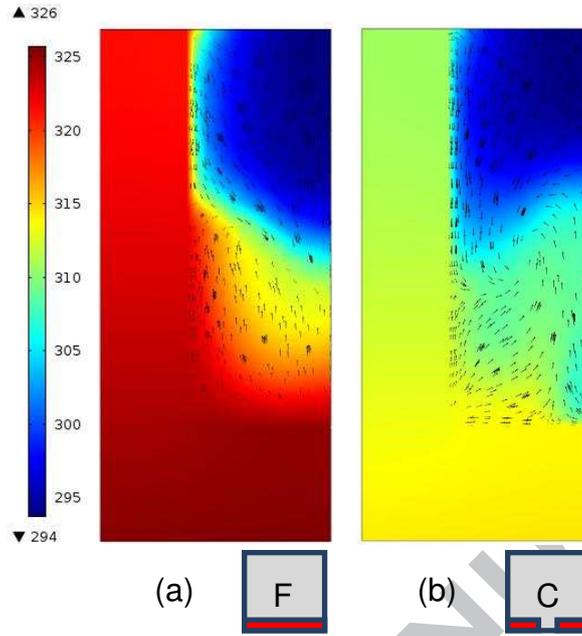
Figure 15: Temperature contours (in K) on a *y-z* plane located 100 μm downstream of the trailing edge of the first VG in the channel: (a) full-span VGs without gap, (b) C-type VGs with a central gap of 100 μm. The arrows indicate *y,z* velocity components at Re=300.
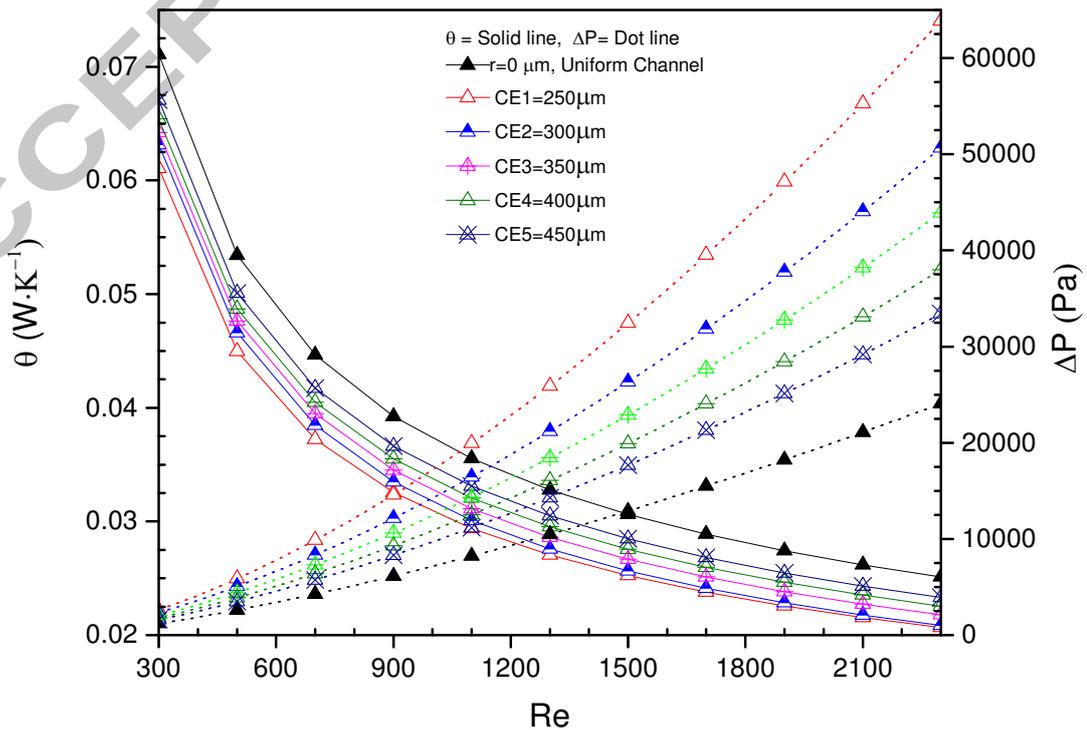
Figure 16: Calculated thermal resistance for CE-type VGs with a gap of 100 μm at each end and a variable width central gap. The width in the legend refers to the combined width of all three gaps.
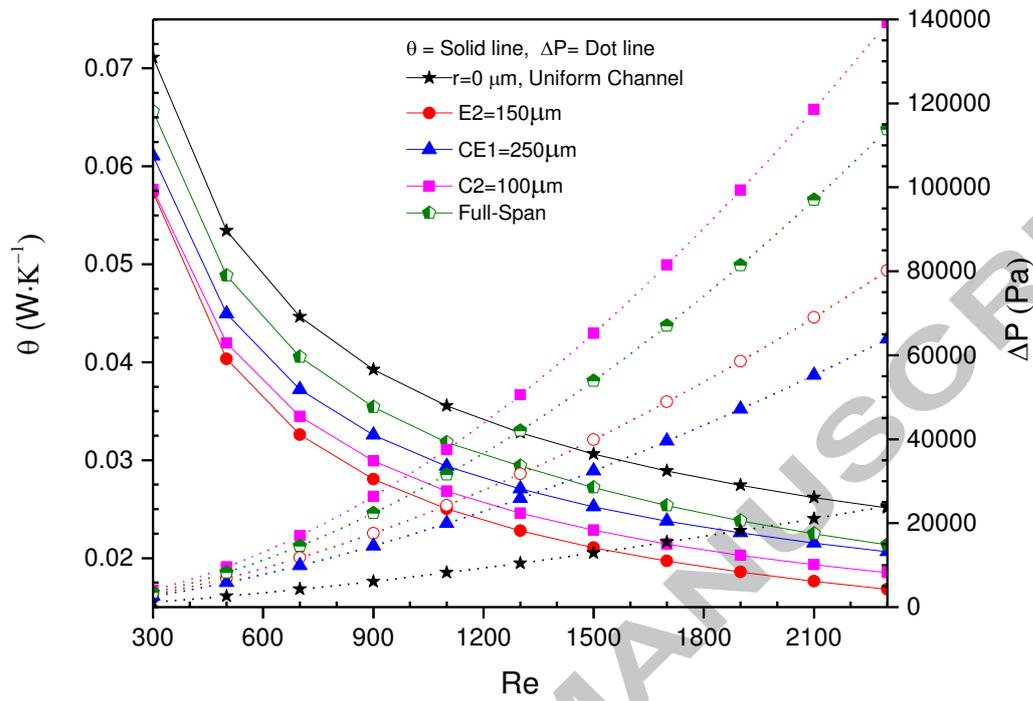
Figure 17: Comparison of the thermal resistances and pressure drops for the 'best' of each VG type.
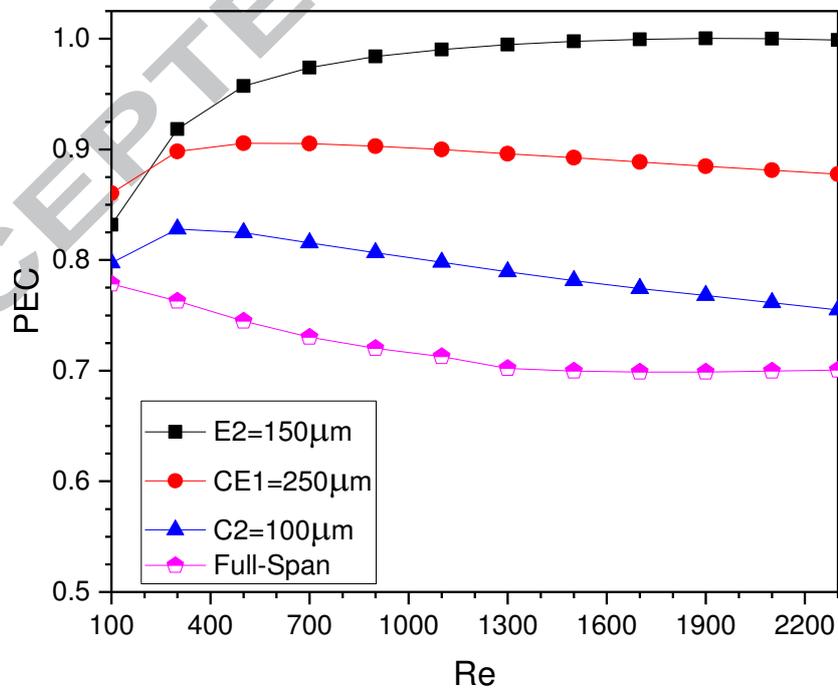
Figure 18: Performance Evaluation Criteria (PEC) index, equation (7), versus Reynolds number for the VGs of each type offering the lowest thermal resistance.
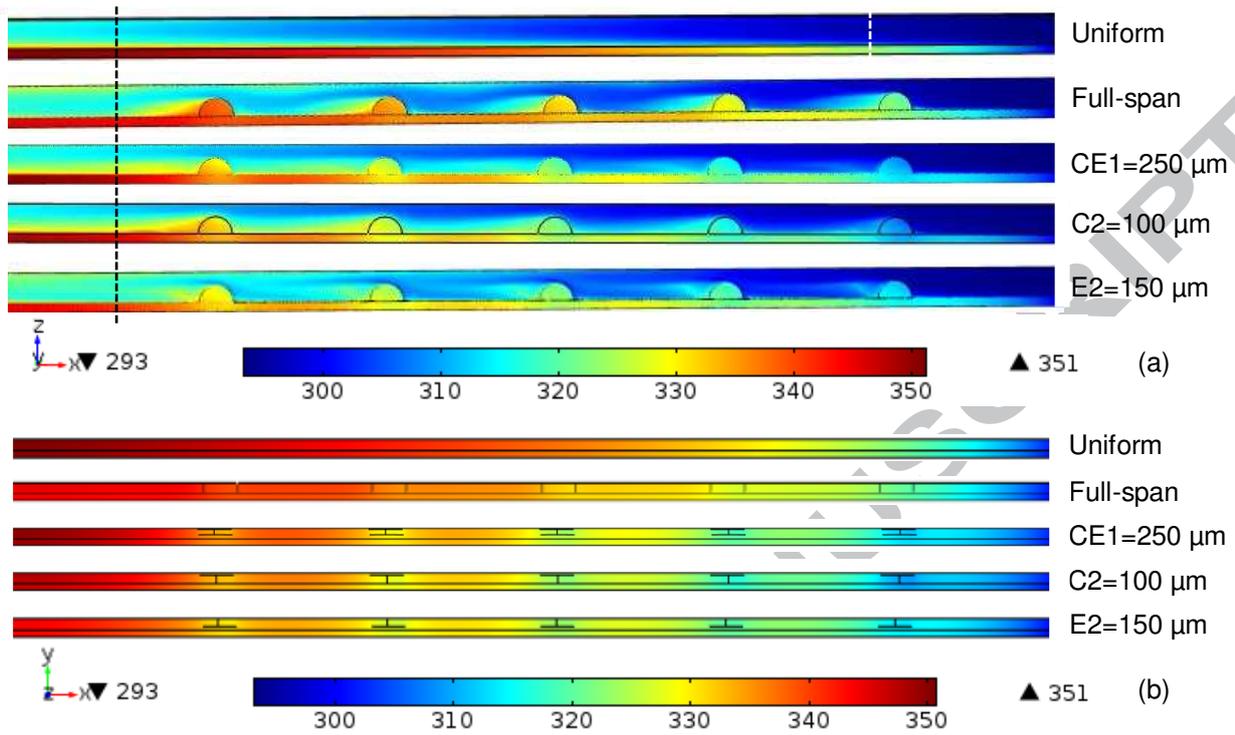
Figure 19: Temperature contours on (a) a plane parallel to the side wall located 100 µm from the wall, and (b) a plane parallel to the solid base located at 2 µm below the fluid flow, for different VG types operating at *Re* = 300. The flow is from right to left.
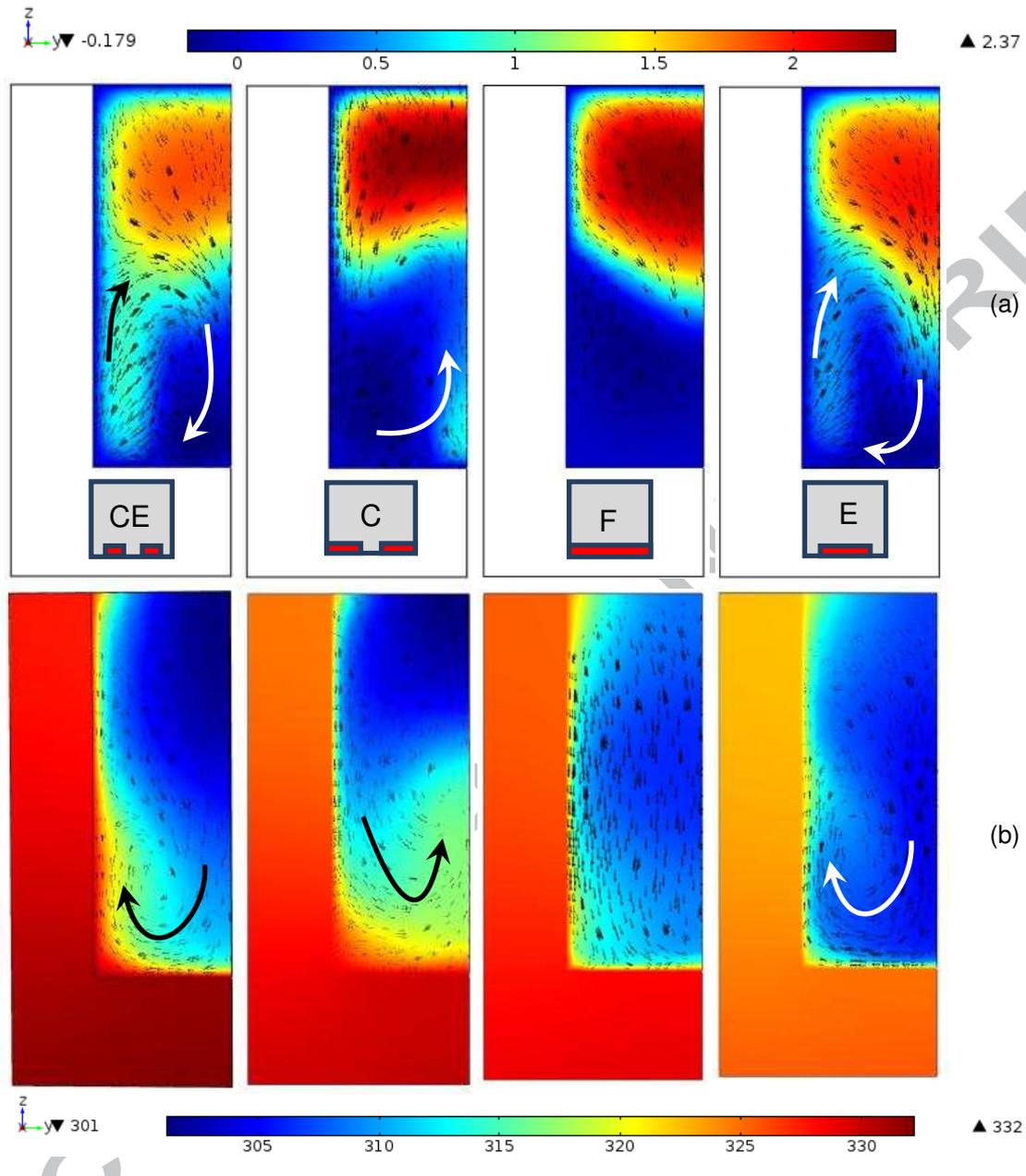
Figure 20: (a) Contours of the *x* component of fluid velocity (in m/s) and *y,z* velocity vectors on a spanwise cross-sectional plane located 100 μm downstream of the first VG; (b) temperature contours and *y,z* velocity vectors on a cross-section located 2000 μm downstream of the centre of the last VG in the channel. The Reynolds number is 500, and the VGs are (from left to right) CE1, C2, full-span, and E2 (see Table 1).
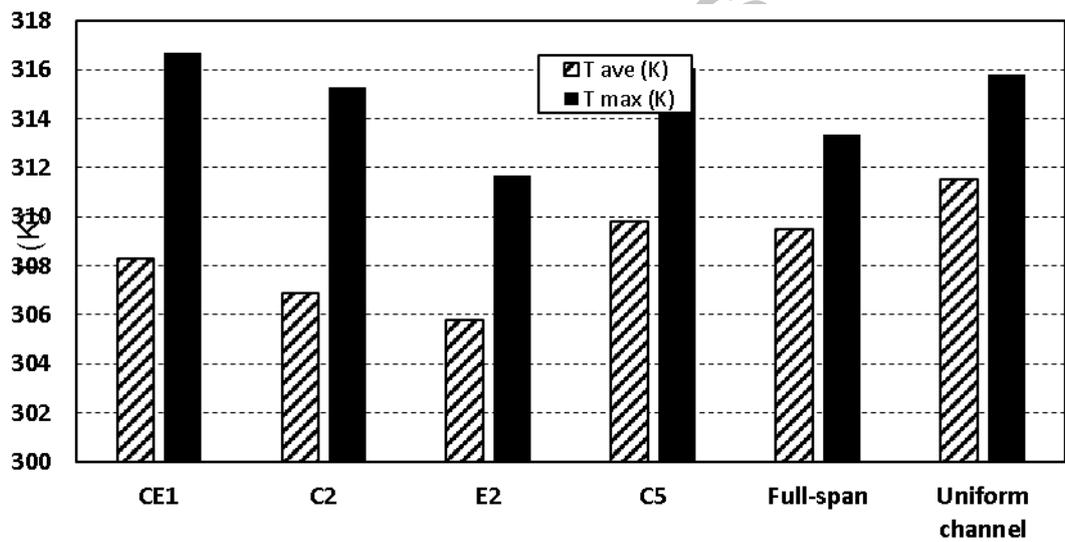
Figure 21: Average and maximum temperatures on the solid base achieved with various vortex generators having spanwise gaps and Reynolds number 1500. See Table 1 for a description of the VG types.

40